eLife

Reviewed Preprint
v2 • August 8, 2024
Revised by authors

Reviewed Preprint
v1 • May 10, 2024

Immunology and Inflammation

SLAM/SAP signaling regulates discrete γδ T cell developmental checkpoints and shapes the innate-like γδ TCR repertoire

Somen K Mistri, Brianna M Hilton, Katherine J Horrigan, Emma S Andretta, Remi Savard, Oliver Dienz, Kenneth J Hampel, Diana L Gerrard, Joshua T Rose, Nikoletta Sidiropoulos, Devdoot Majumdar, Jonathan E Boyson

Department of Surgery, Larner College of Medicine, University of Vermont, Burlington, Vermont 05405, USA • Department of Pathology and Laboratory Medicine, Larner College of Medicine, University of Vermont Medical Center, Burlington, Vermont 05405, USA

Abstract

During thymic development, most γδ T cells acquire innate-like characteristics that are critical for their function in tumor surveillance, infectious disease, and tissue repair. The mechanisms, however, that regulate γδ T cell developmental programming remain unclear. Recently, we demonstrated that the SLAM-SAP signaling pathway regulates the development and function of multiple innate-like γδ T cell subsets. Here, we used a single-cell proteogenomics approach to identify SAP-dependent developmental checkpoints and to define the SAP-dependent γδ TCR repertoire. SAP deficiency resulted in both a significant loss of an immature *Gzma*$^{+}$*Blk*$^{+}$*Etv5*$^{+}$*Tox2*$^{+}$γδT17 precursor population, and a significant increase in *Cd4*$^{+}$*Cd8*$^{+}$ *Rorc*$^{+}$*Ptcra*$^{+}$*Rag1*$^{+}$ thymic γδ T cells. SAP-dependent diversion of embryonic day 17 thymic γδ T cell clonotypes into the αβ T cell developmental pathway was associated with a decreased frequency of mature clonotypes in neonatal thymus, and an altered γδ TCR repertoire in the periphery. Finally, we identify TRGV4/TRAV13-4(DV7)-expressing T cells as a novel, SAP-dependent Vγ4 γδT1 subset. Together, the data suggest that SAP-dependent γδ/αβ T cell lineage commitment regulates γδ T cell developmental programming and shapes the γδ TCR repertoire.

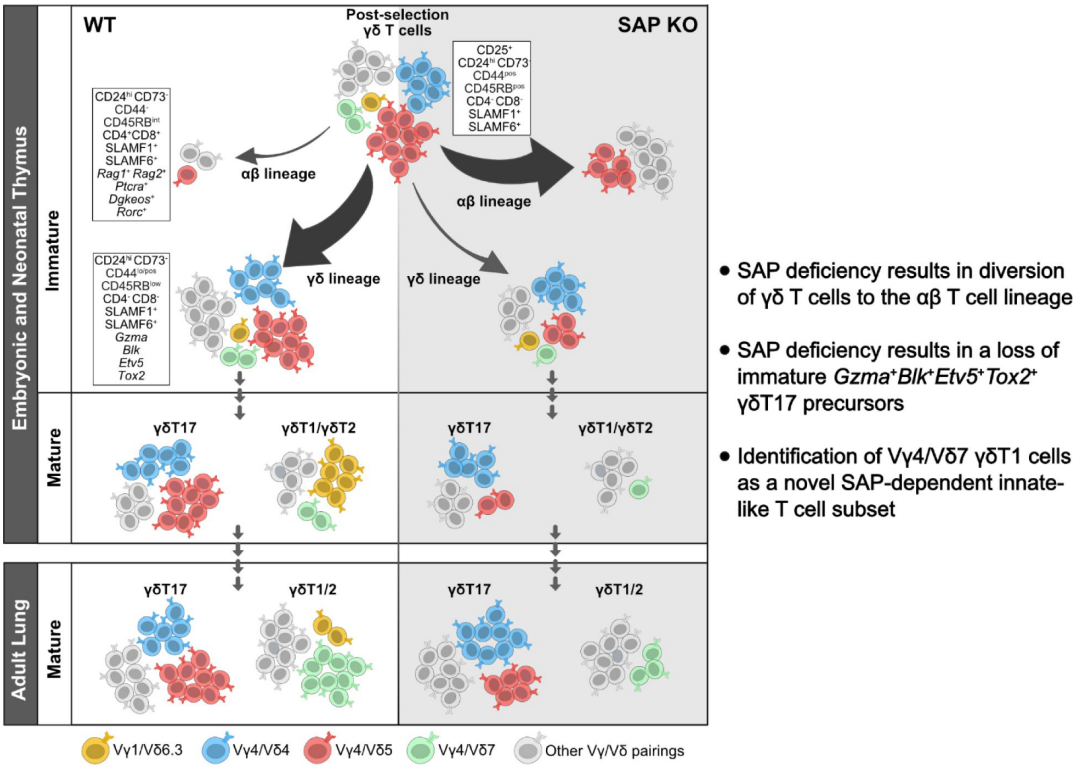

eLife assessment

This **important** study highlights the importance of SLAM-SAP signaling in determining innate gamma-delta T cell sublineages and their T cell receptor repertoires. It uncovers the complex role of the SLAM-SAP pathway in developing specific gamma-delta T cell subsets. The evidence presented is **compelling**, backed by high-quality data obtained through advanced single cell proteogenomics techniques.This work will be of broad interest to immunologists.

https://doi.org/10.7554/eLife.97229.2.sa3

Introduction

Like αβ T cells, γδ T cells can be broadly grouped into innate-like IFN-γ-producing γδT1, IL-4-producing γδT2, or IL-17-producing γδT17 subsets that are functionally programmed during thymic development[1,2,3,4], or inducible subsets that differentiate in the periphery[5]. These innate-like γδ T cells are highly enriched in mucosal tissues such as the skin, gut, and lung and play critical roles in the host response to pathogens, tumor surveillance, autoimmunity, and tissue homeostasis. Accumulating data suggest that the relative balance of these functional γδ T cell subsets can have important implications in disease susceptibility and progression. This is perhaps best exemplified in the setting of cancer where IFN-γ-producing γδT1 have been shown to play a critical role in tumor elimination[6,7,8], while γδT17 subsets promote tumor growth and metastasis[9,10,11,12]. The thymic developmental programs, therefore, that regulate the balance of these functional subsets in the periphery may have considerable impact on disease

outcome. Unlike the case for their αβ T cell counterparts, however, the mechanism that determine whether a developing γδ T cell acquires an innate-like γδT1 or γδT17 phenotype during thymic development remain unclear.

A significant body of data supports a model in which weak or strong TCR signal strength might contribute to the development of innate-like γδT17 (weak signal) and γδT1 (strong signal) subsets[4, 13, 14, 15, 16], and a strong TCR signal has been suggested to be necessary for the development of the IFN-γ and IL-4 producing γδNKT cell subset[17]. However, there is also evidence of a TCR-independent model in which pre-existing hard-wired transcriptional programs regulate the development of some innate-like γδT17 subsets[18], and accumulating data suggest that γδT17 programming is associated with the use of distinct signaling pathways[19, 20, 21].

SLAM family receptors comprise a family of nine receptors, SLAMF1 (SLAM; CD150), SLAMF2 (CD48), SLAMF3 (Ly9; CD229), SLAMF4 (2B4; CD244), SLAMF5 (CD84), SLAMF6 (Ly108; CD352), SLAMF7 (CRACC; CD319), SLAMF8 (BLAME), and SLAMF9 (SF2001; CD84H), that are expressed primarily on hematopoietic cells and which play diverse roles in immune development and function[22]. Most SLAM family receptors interact in a homophilic manner, the exception to this rule being SLAMF4, which serves as the ligand for SLAMF2. SLAM family receptor signals can be both activating or inhibitory, depending on the recruitment of the cytosolic signaling adapter proteins SAP and EAT-2, and inhibitory SHP-1, SHP-2, or SHIP phosphatases to immunoreceptor tyrosine switch motifs in the SLAM family receptor cytoplasmic domain[22]. Although SLAM/SAP signaling has long been known to play a role in innate-like NKT[23] and γδNKT[17] cell development, recent findings from multiple groups demonstrating that this pathway is also involved in the development of innate-like γδT1, γδT17[24] and innate-like MAIT cells[25, 26] indicates that SLAM/SAP signaling plays a fundamental role in the development of a majority of the innate-like T cell lineages.

In this study, we set out to define the stage of thymic development during which SAP mediates its effect on γδ T cell developmental programming and to define SAP-dependent changes in the γδ T cells transcriptional program during their development. Finally, since SAP-dependent innate-like T cell subsets are often characterized by highly restricted TCRs (e.g., $V\gamma1^+/V\delta6.3^+$ γδNKT[27]), we wished to identify whether specific TCR clonotypes were also associated with SAP-dependent γδT1 and γδT17 T cells. Therefore, we utilized a single-cell proteogenomics approach with V(D)J profiling that allowed us to simultaneously compare cell surface protein expression, gene expression, and TCR clonotypes between B6 and $B6.SAP^{-/-}$ γδ T cells from embryonic, neonatal, and adult thymus, as well as from peripheral lung γδ T cells. Collectively, these data provide a comprehensive map of the SAP-dependent γδ T cell subsets and their developmental checkpoints in perinatal and adult thymus.

Results

SLAM family receptor expression marks transcriptionally distinct developmental stages among E17 γδ T cells

γδT17 developmental programming is thought to occur primarily during embryonic/neonatal thymic development[2, 18, 28], and is tightly linked to the expression of discrete TCR gamma and delta pairings[29]. To identify the specific developmental stages of thymic development during which SLAM/SAP signaling pathway exerts its effects, we employed a single-cell RNAseq approach coupled with feature barcoding (i.e., CITEseq[30]) and V(D)J profiling to compare embryonic day 17 (E17) B6 and $B6.SAP^{-/-}$ thymic γδ T cells (**Fig. 1A**). FACS-sorted thymic γδ T cells (**Suppl. Fig. 1**) from individual embryos (n = 4 B6 and 4 $B6.SAP^{-/-}$ mice) were identified using hashtags, and $Vg1^+$ and $Vg4^+$ gd T cells were identified using barcoded antibodies (ADTs). To help define the developmental trajectories of the E17 gd T cells, we also stained cells with

barcoded antibodies specific for CD24, CD73, CD44, and CD45RB, which define distinct developmental pathways of γδT17 and γδT1 cells in the thymus[4, 31, 32], as well as for SLAMF1 and SLAMF6. After data filtering and QC, we verified that clusters were evenly distributed among the biological replicates (**Suppl. Fig. 1**). The resulting dataset represented a total of 5278 thymic γδ T cells from B6 (n = 2597) and B6.SAP$^{-/-}$ (n = 2681) γδ T cells. Data were visualized using uniform manifold approximation and projection (UMAP) for dimensionality reduction and a graph-based clustering approach[33].

First, we annotated the B6 dataset using a combination of cell surface protein expression, gene expression, and TCR clonotype sequence. This analysis revealed 11 B6 E17 γδ T cell clusters, mostly distributed between two major branches (**Fig. 1B**). We observed the presence of CD24^{low}73^{low}44^{high}45RB^{low}SLAMF1^{pos} (c8) and CD24^{low}73^{high}44^{high}45RB^{high}SLAMF6$^{low/pos}$ (c0, c9) clusters, consistent with mature γδT17 phenotype and γδT1 phenotypes, respectively (**Fig. 1C**, **Suppl. Fig. 1**). In support of this annotation, the c8 cluster was enriched in *Il17a*, *Il17f*, *Il23r*, *Rorc*, and TRGV6/TRDV4 (IMGT nomenclature; encoding Vγ6/Vδ1) transcripts with limited CDR3 diversity, while the c0/c9 cluster was enriched in *Ifng*, *Tbx21*, *Klrd1*, *Il2rb*, *Xcl1*, and TRGV5/TRDV4 (encoding Vγ5/Vδ1) transcripts also with little to no diversity (**Figs. 1D – F**, **Suppl. Fig. 2**, **Suppl. Tables 1 and 2**)[34, 35]. Consistent with previous observations[24], we noted that the c0/c9 cluster was highly enriched in *Cd244a* (*Slamf4*), and was enriched in transcripts from another SLAM family member, *Slamf7* (**Figs. 1D - E**). Flow cytometric analysis confirmed that SLAMF7 was expressed primarily on mature γδ T cells and that its expression was mostly confined to γδ T cells expressing the canonical CD44^{+}CD45RB^{+} markers of γδT1 cells (**Suppl. Fig. 1**)[4, 36].

We identified a small CD24$^{low/int}$73^{high}44^{high}45RB^{pos} c3 cluster characterized by enrichment in *Cd200* (whose expression is upregulated upon TCR ligation[37]), *Il2rb*, *Nr4a1*, *Cd244a*, *Xcl1*, and *Tnfrsf9* (encoding 4-1bb receptor). A high frequency of invariant TRGV5/TRDV4 clonotypes and decreased TCR clonotype diversity (**Suppl. Fig. 2**, **Suppl. Table 2)** suggested that c3 represented an immature γδT1 population. The CD24$^{low/pos}$CD73$^{low/pos}$44$^{low/pos}$CD45RB$^{low/pos}$ c4 cluster was enriched in *Ms4a4b and Ms4a6b (*encoding CD20 homologues that modulate T cell activation[38, 39]), *S1pr1*, *Il6ra*, *Cd8a*, *Cd8b1*, and *Ccr9*, suggesting that the c4 cluster represents the previously described emigrating thymic *Ccr9*$^{+}$ *S1pr1*$^{+}$ γδ T cells[40] (**Fig. 1C** **and 1E**). Consistent with the c4 cluster representing naïve emigrating thymic γδ T cells, the diversity of the c4 TCR clonotypes was the highest among the CD24$^{low/int}$ (c0/c9, c8, c3) clusters (**Suppl. Fig. 2**).

We identified several immature CD24^{high}CD73^{neg} ADT clusters (c1, c2, c7, c5, c6, and c10) that also expressed SLAMF1 and/or SLAMF6 (**Fig. 1B** **and Suppl. Fig 1**). The c1 and c2 clusters were enriched in γδT17-associated genes such as *Blk*, *Maf*, *Sox13*, *Ccr2*, *Tcf12, and Rorc*[32, 41, 42, 43, 44], as well as *Sh2d1a* (encoding SAP) and *Ccr9*[16] (**Fig. 1E**, **Suppl. Table 1)**. Within these two clusters, the CD44$^{low/pos}$CD45RB^{low} c2 cluster was especially enriched in genes previously implicated in γδ T cell development such as *Etv5*, *Tox*, *Sox4*, *Tcf7*, *Zbtb16* [44, 45, 46, 47, 48], *Igfbp4* and *Igf1r* which were recently implicated in Th17 differentiation[49], *Tnfsf11* (RANKL) which regulates Aire^{+} mTEC development [50], as well as *Themis* and *Tox2* (**Fig. 1E**, **Suppl. Fig. 1**). A high level of *Gzma* expression identified c2 as the previously described *Gzma*$^{+}$ γδ T cell subset[40]. Interestingly, in addition to expressing γδT17-associated genes, the c2 cluster was also enriched in γδT2-associated *Gata3* and *Il4* transcripts (**Fig. 1D – E**, **Suppl. Table 1**). The CD44$^{low/pos}$CD45RB^{neg} c1 cluster, in contrast, exhibited significantly higher levels of *Il17a*, *Il17f*, *Rorc*, *Maf* [42], as well as *Ifngr1*, consistent with the c1 cluster representing immature γδT17 cells (**Fig. 1D – E**, **1G**, **and Suppl. Fig. 1**).

Analysis of the c1 and c2 TCR transcripts revealed that the c2 cluster was notably enriched in TRGV4-expressing cells and that 87% of Vγ4 T cells utilized just 3 TRDV chains (50% TRDV5, 24% TRDV2-2, and 12% TRAV13-4/DV7) (**Fig. 1F**, **Suppl. Table 2**). Clonotype analysis revealed a high frequency of semi-invariant TRGV4/TRDV5 and TRGV4/TRDV2-2 clonotypes previously associated

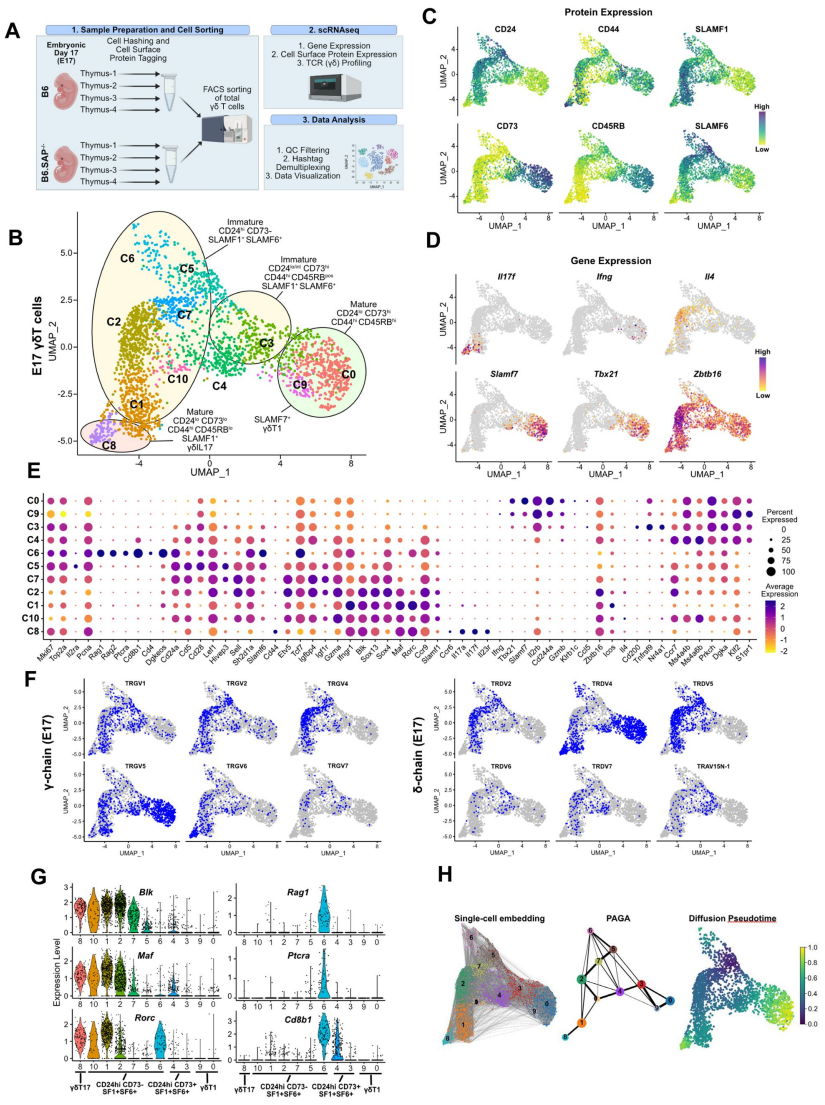

Figure 1.

SLAM family receptor expression marks transcriptionally distinct developmental stages among E17 γδ T cells.

(A) Schematic workflow depicting the methodology for single-cell RNA sequencing (scRNAseq) library preparation and subsequent data analysis pipeline employed in this study. **(B)** Uniform Manifold Approximation and Projection (UMAP) visualization displaying 11 distinct clusters of E17 B6 thymic γδ T cells, n = 4 individual mice. Clusters are annotated based on comprehensive protein and gene expression data. **(C)** Feature plots illustrating the cell surface protein expression profiles of CD24, CD73, CD44, CD45RB, SLAMF1, and SLAMF6 on B6 E17 thymic γδ T cells. Each data point represents a cell, color-coded to indicate varying protein expression levels (high: dark blue, low: yellow). **(D)** Feature plot illustrating the gene expression profiles of signature genes among individual B6 E17 thymic γδ T cells. Each data point represents a cell, color-coded based on gene expression levels (high: purple, low: yellow). **(E)** Dot plot demonstrating the scaled expression levels of selected genes in E17 B6 thymic γδ T cells. Normalized expression levels are depicted using a color scale ranging from low (yellow) to high (purple). Dot size corresponds to the fraction of cells within each cluster expressing the specific marker. **(F)** UMAP representation of E17 B6 thymic γδ T cells indicating the expression of selected TRGV (TCRγ; left) and TRDV (TCRδ; right) chain V-segment usage (in blue) across individual cells. **(G)** Violin plots illustrating the expression patterns of selected genes among E17 B6 thymic γδ T cell clusters. **(H)** Visualization of single-cell trajectories using PAGA (partition-based graph abstraction) with single-cell embedding (left) showing connectivity between individual nodes (middle). Weighted edges represent statistical measures of interconnectivity. The diffusion pseudotime plot (right) delineates inferred pseudotime progression of cells along developmental trajectories using cluster 5 (C5) as the root, highlighting their developmental order (from purple to yellow).

with γδT17[51, 52, 53] (**Suppl. Fig. 2, Suppl. Table 2**). In contrast, the c1 cluster possessed comparatively fewer of these TRGV4 clonotypes, and was enriched in TRGV6, TRGV5, and TRGV1 paired with TRDV4 (**Suppl. Fig. 2, Suppl. Table 2**). Indeed, we noted that the Vγ1 repertoire, which is diverse in adult tissues, was dominated by TRGV1/TRDV4 clonotypes (35% of all TRGV1) in E17 thymus, and just two closely related semi-invariant TRGV1/TRDV4 clonotypes comprised 17.4% of all TRGV1. The location of these clonotypes in the immature γδT17-related clusters (**Suppl. Fig. 2**) suggested that they represent the dominant IL-17-producing Vγ1 clonotypes at E17, which we verified using flow cytometry (**Suppl. Fig. 3**).

Since the IL-4-producing Vγ1/Vδ6.3 γδNKT cell subset develops in fetal thymus[1], we asked whether the *Il4*-enriched γδ T cells in cluster 2 (**Fig. 1D**) were immature Vγ1 γδNKT cells with previously identified canonical Vδ6.3 sequences[27]. Interestingly, while we did identify a small number of Vγ1 T cells with these canonical sequences (encoded by TRAV15-1/DV6-1 or TRAV15N-1) in our dataset, these were not present in the *Il4*-enriched c2 cluster.

The $CD44^{pos}CD45RB^{pos}$ c5 cluster was enriched in *Il2ra, Scin, Bex6, Cd5, Slamf6, Cd28, Hivep3*, and cell-cycle/metabolism genes, consistent with γδ T cells that have recently developed from DN2/DN3[40, 54, 55]. Within the c5 and c7 clusters, we noted that while there was expression of γδT17-associated genes such as *Blk, Maf, Sox13,* and *Etv5*, there was relatively little *Rorc* expression. *Rorc* expression became apparent in the c2 cluster ($Rorc^{low}$) and was significantly increased in the c1 cluster (**Suppl. Fig. 1**). Flow cytometric analysis confirmed BLK and PLZF expression in $CD25^{high}$ E17 Vγ4 T cells, while RORγt expression was primarily observed in the $CD25^{neg}$ population, suggesting that BLK is expressed soon after γδ T cell selection, followed by RORγt (**Suppl. Fig. 3**). These data were consistent with MAF-directed expression of *Rorc*[40, 42] and suggested a c5 – c7 – c2 – c10 / c1 – c8 γδT17 developmental trajectory, which was supported by trajectory inference analysis (**Fig. 1H**).

Finally, analysis of the $CD24^{high}73^{neg}44^{neg}45RB^{int}SLAMF1^{pos}SLAMF6^{pos}$ c6 population revealed that it was highly enriched in *Cd8a, Cd8b1, Cd4, Rag1, Rag2, Ptcra, Arpp21, and Dgkeos,* consistent with cells developing along the αβ T cell lineage (**Figs. 1E, 1G, Suppl. Fig. 1, and Suppl. Table 1**)[56]. Analysis of the Vγ1 and Vγ4 ADTs confirmed that c6 cells were not simply contaminating αβ T cells as both Vγ1- and Vγ4-expressing cells were present in the c6 cluster (**Suppl. Fig. 3**) and analysis of the c6 TCR clonotypes revealed the presence of TRGV1, GV4, GV5, GV6, and GV7 clonotypes, none of which appeared to be specific to the c6 cluster (**Suppl. Table 2**).

Since trajectory inference analysis suggested a strong relationship between the $Il2ra^{+}$ c5 and c6 clusters (**Fig. 1H**), we conducted differential gene expression analysis between the c5 and c6 from B6 mice. Interestingly, we found that the c6 cluster was highly enriched in *Rorc,* suggestive of a γδT17 phenotype, but was mostly lacking in the expression of *Maf, Blk, Ccr2,* and other canonical γδT17-associated transcripts (**Fig. 1E, 1G, and Suppl. Fig. 1**). Indeed, flow cytometric analysis of E17 $TCR\beta^{neg}TCR\delta^{pos}$ γδ T cells confirmed that CD4CD8 DP γδ T cells exhibited an immature $CD44^{low}CD25^{low}MAF^{neg}BLK^{neg}ROR\gamma t^{pos}$ phenotype (**Suppl. Fig. 3**), and that RORγt expression in the absence of BLK or MAF is a characteristic of Lin^{neg} DN thymocytes as they progress from $CD44^{low}25^{high}$ DN3 to $CD44^{low}25^{low}$ DN4 (**Suppl. Fig. 3**). Together, these data suggested that the c6 cluster γδ T cells represented previously described CD4CD8 DP γδ T cells that were developing along an alternative αβ T cell pathway[57, 58, 59].

SAP regulates γδ T cell clonotype diversion into both the γδT17 and the αβ T cell developmental pathways

To identify SAP-dependent developmental checkpoints, we next compared the hashtag-separated B6 and $B6.SAP^{-/-}$ E17 γδ T cell datasets. A comparison of the cluster frequencies between B6 and $B6.SAP^{-/-}$ γδ T cells revealed significantly decreased frequencies of the $CD24^{high}73^{neg}44^{int}45RB^{int}SLAMF1^{pos}SLAMF6^{pos}$ c2 and c1 clusters in $B6.SAP^{-/-}$ mice, and a

striking increase in the frequency of the CD24^{high}73^{neg}44^{neg}45RB^{neg}SLAMF1^{high}SLAMF6^{high} c6 cluster (**Fig. 2A**). A comparison of differentially expressed genes among the immature (c1, c2, c7, c5, c6, and c10) clusters using pseudobulk analysis revealed 234 differentially expressed genes with a p_{adj} threshold < 0.005 and log_2 fold change greater than 0.5, with 148 genes exhibiting decreased expression in B6.SAP$^{-/-}$ γδ T cells, and 86 genes exhibiting increased expression (**Fig. 2B**, **Suppl. Table 3**). Consistent with the decreased frequencies of the c1/c2 clusters in B6.SAP$^{-/-}$ mice, a significant fraction of the differentially expressed genes that were down-regulated in B6.SAP$^{-/-}$ mice reflected γδT17-associated genes (e.g., *Maf, Blk, Ccr2, Sox13, Etv5, etc.*) that were present in the c2 and c1 clusters, as well as a number of c1/c2-enriched genes (e.g., *Cpa3, Tox2, Pdcd1, Tmem121, Bex6*, and *Scin*) whose importance in γδ T cell development is unclear (**Fig. 2B-C**, **Suppl. Table 2**). This was not solely due to the decreased frequency of the c2 and c1 clusters in B6.SAP$^{-/-}$ mice, as a closer analysis revealed a decreased number of transcripts for many signature genes (e.g., *Blk*, *Etv5*, *Ccr2*) prevalent in the c2 cluster and to a lesser extent the c7 cluster (**Suppl. Fig. 4**). Given the decreased expression of *Blk*, we also examined the expression of Src tyrosine kinase family members *Lck* and *Fyn*, which have previously been implicated in T cell development[60]. Unlike *Blk*, which was mostly restricted to γδT17 clusters, *Lck* and *Fyn* expression was more broadly distributed (**Suppl. Fig. 1**). Using pseudobulk analysis to compare their expression between B6 and B6.SAP$^{-/-}$ immature E.17 γδ T cells, we found that neither *Lck* nor *Fyn* expression was appreciably altered (**Suppl. Fig. 4**), suggesting that *Blk* expression was uniquely dependent on SAP. We did note, however, that the magnitude of *Lck* differential expression was close to the 0.5 log_2 FC cut-off and that its expression was increased in B6.SAP$^{-/-}$ γδ T cells (**Suppl. Fig. 4**). Indeed, a large number of genes whose expression was increased in B6.SAP$^{-/-}$ mice were those whose expression was mostly confined to the c6 cluster (e.g., *Cd4, Cd8b1, Ptcra, Rag2*) or whose expression was highest in c6 (e.g., *Tcf7, Thy1, Lck*) (**Fig. 2B-C**, **Suppl. Fig. 4**). Together, these data identified the *Gzma*$^{+}$*Etv5*$^{+}$*Sox13*$^{+}$*Blk*$^{+}$*Tox2*$^{+}$c2 and *Cd4*$^{+}$*Cd8b1*$^{+}$*Ptcra*$^{+}$*Rag2*$^{+}$c6 clusters as SAP-dependent developmental checkpoints.

Next, we asked whether these SAP-dependent alterations in γδ T cell development were associated with any changes in the TCR repertoire. A comparison of all γδ TCR clonotypes between E17 B6 and B6.SAP$^{-/-}$ γδ T cells revealed no significant changes in overall clonotype frequency (**Fig. 2D**). However, a closer examination of TCR repertoire revealed significant changes in the distribution of specific TCR clonotypes. For example, within the TRGV4 repertoire, which represents the dominant TCR among immature clusters at E17, we observed a significant decrease in TRGV4/TRDV5 clonotypes in the c2 cluster and a concomitant increase of these clonotypes in the c6 cluster (**Fig. 2E**). Among the TRGV4 clonotypes, this appeared to be specific to the TRDV5 clonotypes, as we observed no significant differences c2 and c6 frequencies among TRGV4/TRDV2-2 and TRDV7 clonotypes (**Fig. 2E**). We did note, however, a significant increase in the TRGV4/TRDV7 clonotypes in the *Il2ra*$^{+}$ c5 cluster (**Fig. 2E**). Within the TRGV1 repertoire, we noted a significant increase in TRGV1/TRDV4 clonotypes within the c6 cluster (**Fig. 2E**). Together, these data suggested that SAP operated at an early stage of γδ T cell development during or soon after the down-regulation of *Il2ra,* and that it positively regulated entry into the γδT17 pathway at the c5/c7 to c2 transition, while at the same time inhibiting entry into the CD4^{+}CD8^{+} αβ T cell-like c6 cluster. The net result of these changes appeared to be that specific TCR clonotypes such as TRGV4/TRDV5 were diverted from the γδT17 pathway into the αβ T cell-like pathway.

SAP deficiency is associated with increased numbers of immature CD4^{+}CD8^{+}RORγt^{+} thymic γδ T cells

Next, we independently evaluated these observations using flow cytometry. This analysis revealed that while SAP deficiency did not affect the overall number of E17 γδ T cells (**Suppl. Fig. 5**), it did result in a significant decrease of immature CD24^{pos}BLK^{pos}MAF^{pos}RORγt^{pos} γδ T cells in E17 B6.SAP$^{-/-}$ thymus (**Fig. 3A-B**). We found that this decrease was most pronounced in the CD44^{pos} population after downregulation of CD25 (**Fig 3A**, **Suppl. Fig. 5**) and that this population exhibited a high level of PLZF expression, suggesting it corresponded to the

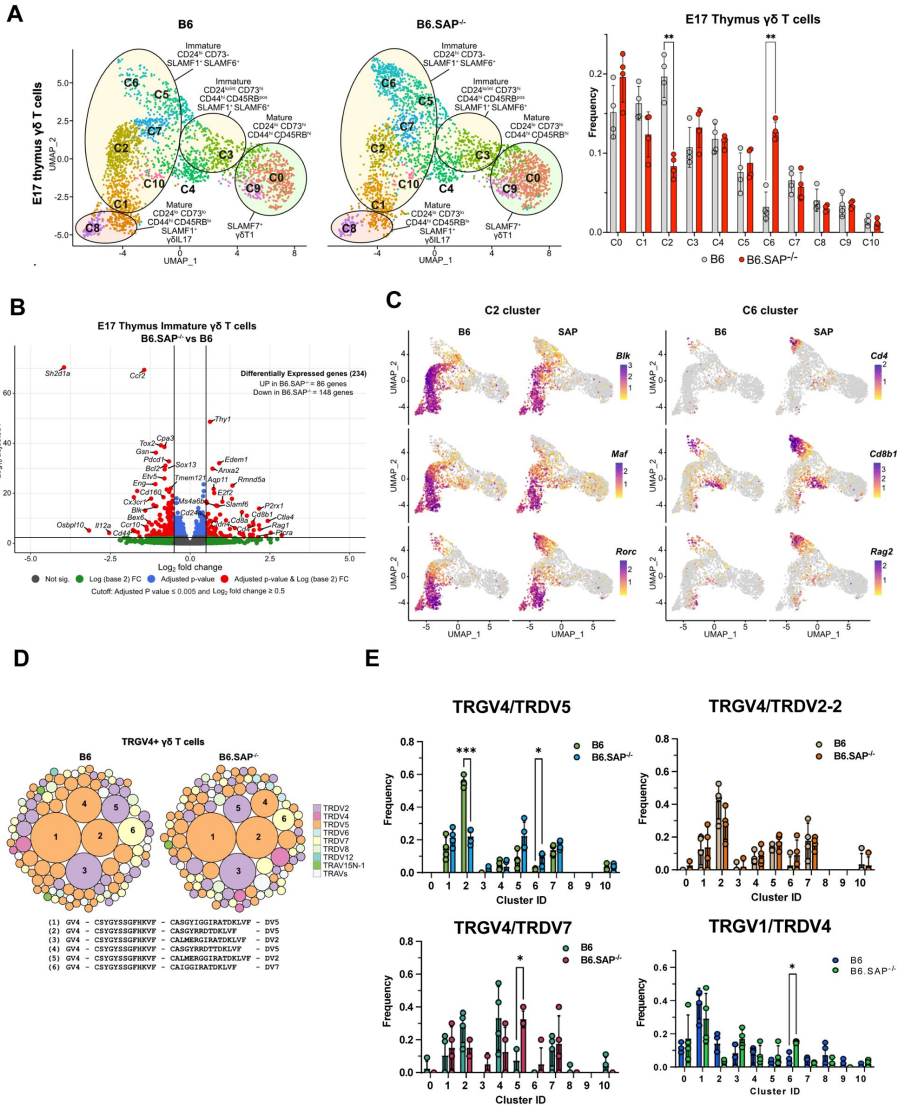

Figure. 2.

Identification of SAP-dependent developmental checkpoints during E17 γδ T cell developmental programming.

(A) UMAP representation of B6 (left) and B6.SAP$^{-/-}$ (right) γδ T cells from E17 thymi (n = 4 mice per group) is shown at *left.* Clusters were annotated based on protein and gene expression data. The frequencies of B6 and B6.SAP$^{-/-}$ E17 γδ T cell clusters is shown at right. Bars represent the mean cluster frequency, error bars represent standard deviation, **p ≤ 0.01, two-way ANOVA, Sidak multiple-comparisons test; n=4 mice/genotype. **(B)** Volcano plot of differentially expressed genes among immature CD24^{high}CD73^{neg} (clusters: C1, C2, C5, C6, C7, and C10) B6 and B6.SAP$^{-/-}$ γδ T cells using pseudobulk scRNAseq analysis. Genes exhibiting a $log_2FC \geq 0.5$ or ≤ −0.5, and a $p_{adj} \leq 0.005$ in are shown in red. Only some selected genes are labelled for the sake of clarity. **(C)** Feature plots illustrating gene expression profiles of selected C2 and C6 cluster-specific genes among individual B6 and B6.SAP$^{-/-}$ E17 thymic γδ T cells. Each point represents a cell, color-coded by gene expression level (high: purple, low: yellow). **(D)** TCR clonotype bubble plot displaying the top 100 B6 and B6.SAP$^{-/-}$ TRGV4 clonotypes in E17 thymus. Bubbles represent unique TRGV4/TRDV clonotypes; size indicates frequency of clonotype among all Vγ4 T cells (n = 388 B6, 288 B6.SAP$^{-/-}$ cells), and colors denote specific TRDV chains utilized. Selected clonotypes are numbered and their respective CDR3γ and CDR3δ sequences displayed below. Data are **(E)** Altered TRGV/TRDV clonotype distribution between B6 and B6.SAP$^{-/-}$ E17 thymic γδ T cells. Frequencies of selected clonotypes among different clusters of B6 and B6.SAP$^{-/-}$ E17 γδ T cells is shown. Bars represent the mean clonotype frequency among the indicated TRGV/TRDV pairings shown, error bars represent standard deviation, *p ≤ 0.05, ***p ≤ 0.001, two-way ANOVA, Sidak multiple-comparisons test; n = 4 mice/genotype-age groups.

CD44^{+}*Blk*$^{+}$*Maf*$^{+}$*Zbtb16*$^{+}$*Rorc*$^{+}$ c1 cluster (**Suppl. Fig. 5**). In addition, UMAP analysis of E17 Vγ4 T cells flow cytometric data revealed the presence of a SAP-dependent CD24^{pos}BLK^{pos}PLZF^{pos}RORγt^{neg} population in B6.SAP$^{-/-}$ thymus (**Suppl. Fig. 5**) consistent with the phenotype of the *Rorc*^{low} c2 cluster. In contrast, we found no evidence of a SAP-dependent decrease in the CD25^{pos} population frequency, consistent with the notion that SAP exerts its effect during or after this stage of development (**Fig. 3A**). We also noted that in addition to its effect on the numbers of immature thymic γδT17, SAP deficiency resulted in the reduced expression levels of some of these markers, most notably BLK (**Fig. 3C**), a finding that was consistent with the decreased number of *Blk* transcripts observed in **Fig. 2**. Interestingly, as PLZF induction is often associated with SLAM/SAP signaling, we noted that SAP did not affect overall PLZF expression levels in E17 thymic γδ T cells (**Suppl. Fig. 5**).

In contrast to the decreased numbers of CD24^{pos}BLK^{pos}MAF^{pos}PLZF^{pos} RORγt^{pos} γδ T cells, we observed a significant increase in the frequency and number of CD24^{pos}BLK^{neg}MAF^{neg}PLZF^{neg}RORγt^{pos} γδ T cells (**Figs. 3A-B**), whose phenotype was consistent with the αβ T cell-like c6 cluster in **Fig. 2**. Consistent with our finding that the c6 cluster was enriched in CD4 and CD8, we found that the frequency and number of CD4 and CD8-expressing CD24^{pos} TCRδ^{pos}TCRβ^{neg} BLK^{neg}MAF^{neg}RORγt^{pos} thymic γδ T cells was significantly increased in B6.SAP$^{-/-}$ mice (**Fig. 3D**). Together, these analyses confirmed our single-cell CITEseq analysis, and suggested that SAP regulated both the throughput of immature γδ T cells in the γδT17 cell pathway as well as the αβ T cell-like pathway. More specifically, the data suggested that SAP promoted progression to the CD24^{pos} BLK^{pos}MAF^{pos}PLZF^{pos}RORγt^{low} c2 cluster that is enriched in a number of genes (e.g., *Sox13, Etv5, Blk, Maf)* known to regulate γδT17 development, but that it inhibited entry into the CD24^{pos}44^{neg}BLK^{neg}MAF^{neg}RORγt^{pos} αβ–T cell-like pathway (c6 cluster).

Identification of SAP-dependent developmental checkpoints during neonatal and adult thymus γδ T cell developmental programming

The neonatal period is a time of rapid expansion of numerous γδ T cell subsets in the thymus including Vγ4 γδT17 and γδNKT. Therefore, we conducted a comparison between B6 and B6.SAP$^{-/-}$ neonatal and adult thymic γδ T cells, to identify novel SAP-dependent developmental checkpoints and to track the outcome of the SAP-dependent alterations in γδ T cell development observed in E17 thymus. Neonate datasets revealed a similar branched clustering pattern as in E17 with some notable differences. Similar to E17, we observed immature CD24^{pos}73^{low}SLAMF1^{pos}SLAMF6^{pos} clusters (c0, c1, c2, c3, c9, c12, c14), CD24^{pos}73$^{low/pos}$SLAMF1^{pos}SLAMF6^{pos} (c4, c5, c10, c15) *S1pr1*-enriched “naïve” clusters, mature CD24^{neg}73^{low}SLAMF1^{pos}SLAMF6^{neg} (c6, c7) gdT17 clusters, and a mature CD24^{neg}73^{pos}SLAMF1^{neg}SLAMF6$^{low/pos}$*Slamf7*^{high} (c8) gdT1 cluster (**Fig. 4A-B**, **Suppl. Fig. 6**). In general, we noted good correlation with cluster-specific gene expression between the E17 and D9 (Day 9) datasets. A notable exception was a striking decrease in *Zbtb16* expression among all immature neonatal γδ T cells, which is consistent with previous reports[16], [40] (**Suppl. Fig. 6**, **Suppl. Table 3**).

In contrast to the E17 dataset, the neonatal thymic γδ T cell dataset contained a CD24^{neg}73^{pos}SLAMF1^{neg}SLAMF6^{high}*Slamf7*^{neg} (c13) γδT2 cluster enriched in *Il4*, *Il13*, *Zbtb16*, *Cd40lig*, and *Nos1* (**Suppl. Fig. 6**, **Suppl. Table 1)**, suggesting it represented IL-4-producing γδNKT cells. Indeed, examination of the γδT2 (c13) and γδT1 (c8) cluster TCR repertoires revealed a significant enrichment of canonical TRGV1 and TRAV15N-1 or TRAV15-1/DV6-1 sequences characteristic of γδNKT cells (**Fig. 4C**, **Fig. 5**)[27]. Analysis of the differentially expressed genes in the γδT1 (c8) and γδT2 (c13) clusters revealed that *Zbtb16*, *Icos,* and *Slamf6* were markers of γδT2 cells while *Tbx21*, *Klrb1c* (NK1.1), and *Slamf7* were markers of γδT1 cells in neonatal thymus (**Suppl. Fig. 6**). Flow cytometric analysis confirmed that PLZF^{hi} γδT2 Vγ1Vδ6.3 cells co-express SLAMF6 and ICOS while Tbet^{hi} γδT1 Vγ1Vδ6.3 cells are NK1.1^{+} and are either SLAMF6^{-}SLAMF7^{+} or SLAMF6^{+}SLAMF7^{+} (**Suppl. Fig. 7**).

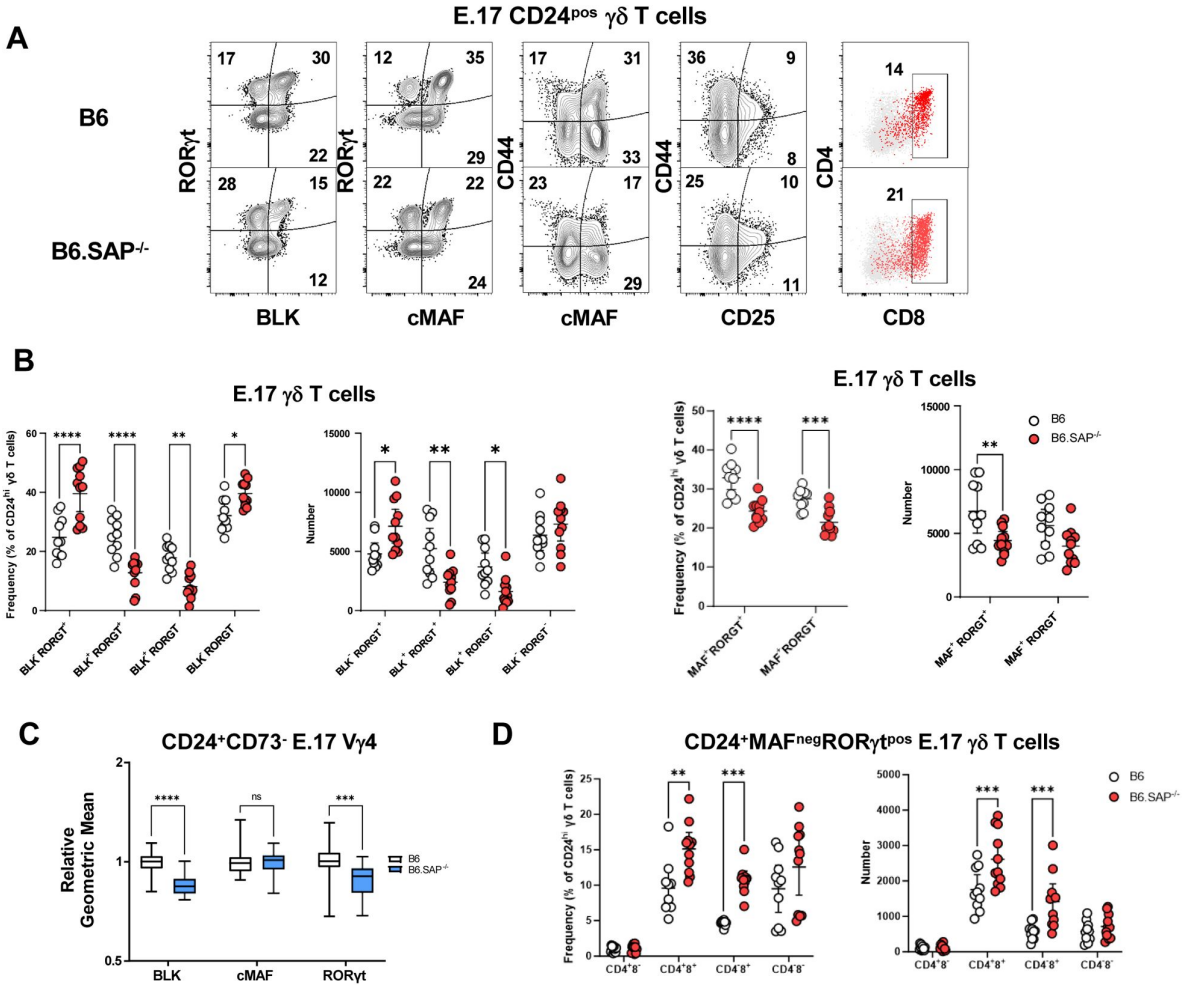

Figure 3.

Increased frequency and numbers of immature CD4^{+}CD8^{+}c-MAF^{-}RORγt^{+} thymic γδ T cells in B6.SAP$^{-/-}$ E17 γδ T cells.

(A) Representative contour plots depicting CD24^{pos} E17 γδ T cells in B6 (top) and B6.SAP$^{-/-}$ (bottom) mice. Concatenated data from 2 B6 and 3 B6.SAP$^{-/-}$ embryos are shown, and are representative of 2 independent experiments. Numbers in the plots represent the frequency as a percentage of CD24^{pos} γδ T cells. **(B)** Cumulative frequency and number of immature CD24^{pos} BLK- (left), c-MAF- (right), RORγt-expressing E17 thymic γδ T cells. The mean and standard deviation are indicated. Data are the cumulative data from 2 independent experiments, n = 10 B6, 11 B6.SAP$^{-/-}$ pooled embryonic thymi, *p ≤ 0.05, **p ≤ 0.01, ***p ≤ 0.001, ****p ≤ 0.0001, two-way ANOVA, Sidak's multiple comparisons test. **(C)** Relative geometric mean of BLK, c-MAF, and RORγt expression in B6 and B6.SAP$^{-/-}$ E17 CD24^{+}CD73^{-} Vγ4 γδ T cells, *p ≤ 0.001, ****p ≤ 0.0001, two-way ANOVA, Sidak's multiple comparisons test. Data are representative of 2 independent experiments, 7-9 mice per group. **(D)** Cumulative frequency (left) and number (right) of immature CD4- and CD8-MAF^{neg}RORγt^{pos} E17 thymic γδ T cells in B6 and B6.SAP$^{-/-}$ thymus. The mean and standard deviation are indicated. Data are the cumulative data from 2 independent experiments, n = 10 B6, 11 B6.SAP$^{-/-}$ pooled embryonic thymi, **p ≤ 0.01, ***p ≤ 0.001, ****p ≤ 0.0001, two-way ANOVA, Sidak's multiple comparisons test.

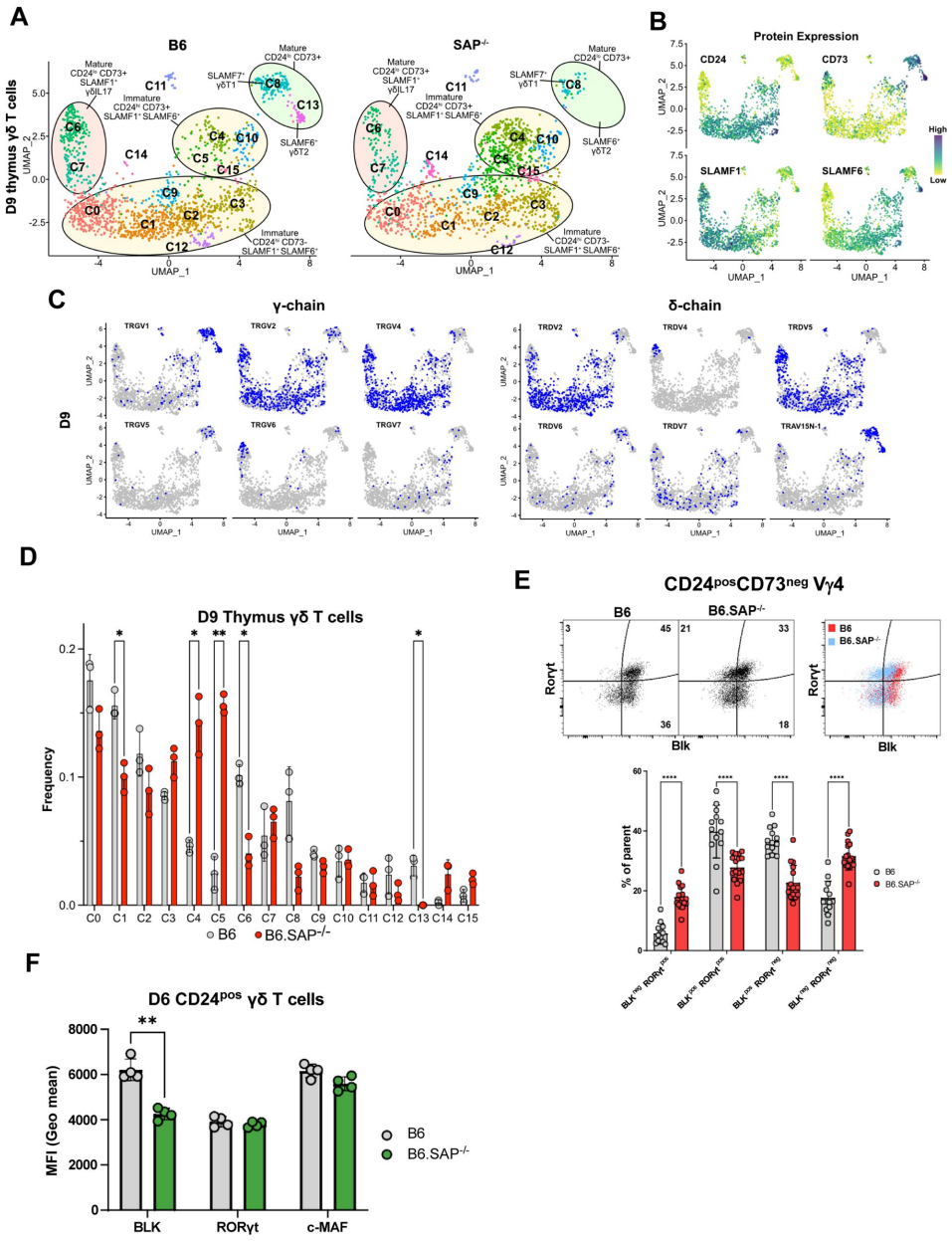

Figure 4.

Identification of SAP-dependent developmental checkpoints during neonatal γδ T cell developmental programming.

(A) UMAP representation of B6 (left) and B6.SAP$^{-/-}$ (right) γδ T cells from D9 neonatal thymi (n = 3 mice per strain). Cluster annotation is based on comprehensive protein and gene expression data. **(B)** Feature plots displaying cell surface protein expression patterns of CD24, CD73, SLAMF1, and SLAMF6 on D9 B6 thymus γδ T cells. Data are color-coded based on protein expression level (high: dark blue, low: yellow). **(C)** UMAP representation of D9 B6 thymic γδ T cells exhibiting selected TRGV4 (left) and TRDV (right) chain V-segment usage (in blue) in individual cells. **(D)** Frequencies of B6 and B6.SAP$^{-/-}$ D9 thymic γδ T cell clusters. Bars represent the mean cluster frequency, error bars represent standard deviation, *p ≤ 0.05, **p ≤ 0.01, two-way ANOVA, Sidak multiple-comparisons test, 3 mice/strain. **(E)** Representative contour plots depicting BLK and RORγt expression in B6 and B6.SAP$^{-/-}$ CD24^{pos}CD73^{neg} D9 Vγ4 T cells are shown *above*. Cumulative frequencies of BLK and RORγt expression are shown *below*. The mean and standard deviation are indicated. Data are the cumulative data from 3 independent experiments, n = 13 B6, 16 B6.SAP$^{-/-}$ mice, ****p ≤ 0.0001, two-way ANOVA, Sidak's multiple comparisons test. **(F)** Decreased BLK expression in immature B6.SAP$^{-/-}$ γδ T cells. Data represent the mean expression of the indicated proteins in D6 neonate BLK^{pos}, RORγt^{pos}, or c-Maf^{pos} thymic γδ T cells, **p ≤ 0.01.

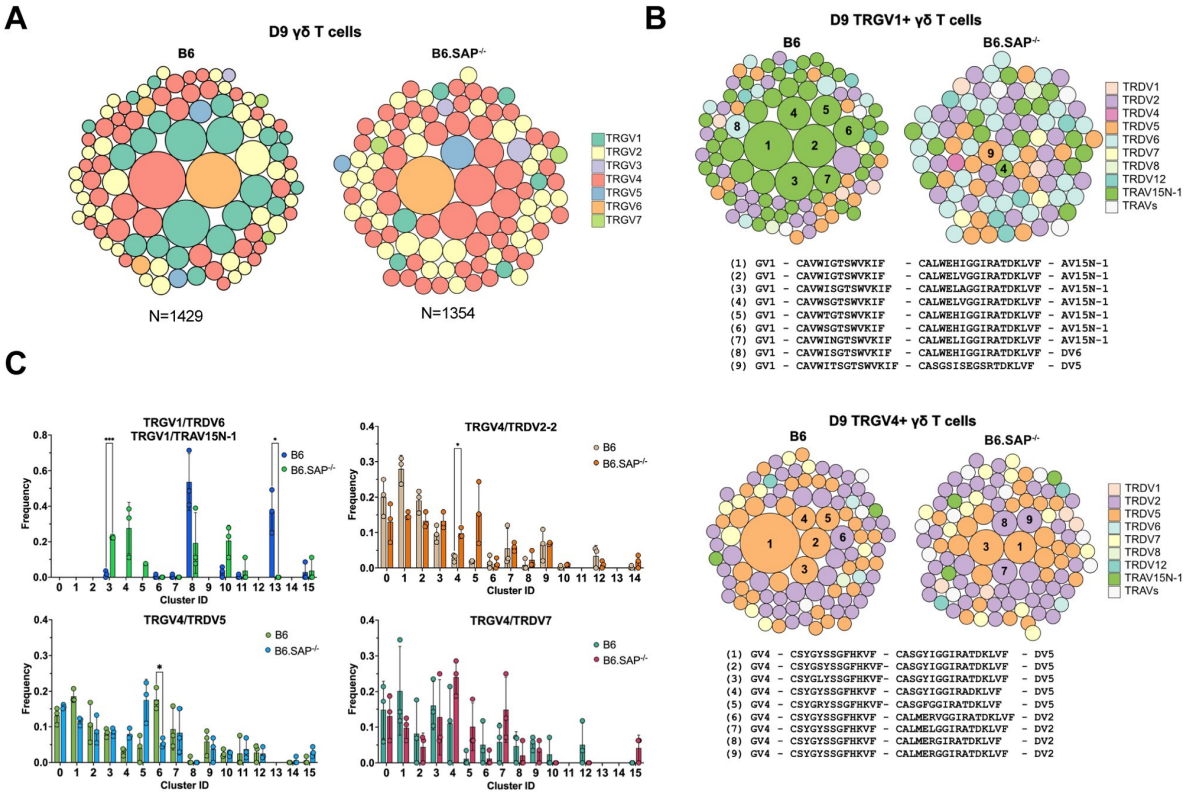

Figure 5.

SAP shapes the neonatal γδ TCR repertoire.

(A) TCR clonotype bubble plots depicting the top 100 B6 and B6.SAP$^{-/-}$ TCR clonotypes among D9 thymic γδ T cells. Each bubble represents a unique clonotype, is sized according to its frequency as a percentage of all γδ T cells n = 1429 B6, 1354 B6.SAP$^{-/-}$ cells), and is colored based on specific TRGV chains utilized. **(B)** TCR clonotype bubble plots depicting the top 100 B6 and B6.SAP$^{-/-}$ TRGV1 (*above*) and TRGV4 (*below*) clonotypes among D9 γδ T cells. Bubble size indicates clonotype frequency as a percentage of TRGV1^{+} (n = 198 B6, 98 B6.SAP$^{-/-}$) or TRGV4^{+} (n = 646 B6, 669 B6.SAP$^{-/-}$) cells, and colors correspond to specific TRDV chains. Selected clonotypes are numbered and their corresponding CDR3γ and CDR3δ sequences are displayed below. **(C)** Distribution of selected TRGV/TRDV clonotypes among B6 and B6.SAP$^{-/-}$ D9 thymic γδ T cell clusters. Data representative of 3 mice/strain, *p ≤ 0.05, ***p ≤ 0.001, two-way ANOVA, Sidak multiple-comparisons test.

A comparison of B6 and B6.SAP$^{-/-}$ neonatal gd T cells revealed multiple SAP-dependent changes in clustering. Among the immature γδ T cells, we observed a decreased frequency of the immature CD24^{high}73^{neg}SLAMF1^{pos}SLAMF6^{pos} c1 cluster (**Fig. 4D**) that was enriched in *Blk, Etv5, Sox13, Rorc,* and *Maf* (**Suppl. Fig. 6**), suggesting it was analogous to the SAP-dependent c2 cluster in E17 γδ T cells. Similar to our observations in E17 γδ T cells, flow cytometric analysis confirmed both a decrease in BLK^{pos}RORγt^{pos} and BLK^{pos}RORγt^{neg} γδ T cell populations, as well as a decreased level of BLK expression (**Fig. 4E-F**). In addition, we observed an increased frequency of immature CD24^{high}73^{neg}SLAMF1^{pos}SLAMF6^{pos} cluster with characteristics of αβ T cells (c14) in B6.SAP$^{-/-}$ D9 thymic γδ T cells (**Fig. 4D**, **Suppl. Fig. 6**). While this increase did not reach the level of significance, presumably due to the very low number of c14 cells in the dataset, flow cytometric analysis revealed a significant increase in immature CD24^{pos}73^{neg}BLK^{neg}RORgt^{pos} gd T cells, a phenotype consistent with gd T cells that have been diverted to the ab developmental pathway (**Fig. 4E**). Last, we observed an increased frequency of immature CD24^{pos}73$^{low/pos}$ SLAMF1^{pos}SLAMF6^{pos} *S1pr1*-enriched c4 and c5 clusters, but not the closely related *Cd200*-enriched c10 cluster (**Fig. 4D**). While we did confirm an increased number of CD200^{neg}S1pr1^{pos} γδ T cells in neonatal thymus by flow cytometry, this increase was relatively small and its significance is unclear (**Suppl. Fig. 7**). Independent confirmation of these SAP-dependent changes in neonatal γδ T cell gene expression was obtained by conducting bulk RNAseq analysis of FACSs-sorted CD24^{high} neonatal thymic γδ T cells from B6 and B6.SAP$^{-/-}$ mice (**Suppl. Table 4**).

Among the mature neonatal γδ T cells, we observed a decreased frequency of the CD24^{low}73^{neg}SLAMF1^{pos}F6^{low} γδT17 c6 cluster, which was consistent with our previous observation of decreased IL-17 production in B6.SAP$^{-/-}$ neonatal γδ T cells[24]. Interestingly, we observed a striking loss of the CD24^{low}73^{high}SLAMF1^{low}F6^{high}F7^{neg} γδT2 c13 cluster in B6.SAP$^{-/-}$ mice, as well as a decreased frequency of the mature CD24^{low}73^{high}SLAMF1^{low}F6^{low}F7^{high} γδT1 c8 cluster (**Fig. 4A - D**). These findings were consistent with a SAP-dependent loss of both the IL-4- and IFN-γ-producing γδNKT as well as non-γδNKT γδT1 cells (discussed further below). Unfortunately, while we were able to define mature SAP-dependent γδNKT subsets, we found no evidence of immature γδNKT cells in our dataset, suggesting that they develop during a brief developmental window between E17 and D9 after birth.

A comparison of B6 adult thymic γδ T cells between B6 and B6.SAP$^{-/-}$ mice recapitulated many of our observations of the neonatal thymus, although to a somewhat lesser degree. For example, we observed a small but significant decrease in the frequency of the CD24^{high}CD73^{low} adult thymic c1 and c2 clusters in B6.SAP$^{-/-}$ mice that was coupled with an increased frequency of the CD24^{pos}CD73$^{+/-}$ c0 cluster (**Suppl. Fig. 8**). Like the SAP-dependent E17 c2 and D9 c1 clusters, the adult thymus c1 and c2 clusters were enriched in γδT17-associated *Blk, Etv5, Sox13, Maf,* and *Rorc* (mostly in c2) indicating that SAP regulates this γδ T cell thymic developmental checkpoint at all ages. Likewise, both the adult thymus c0 and the neonatal c4 and c5 clusters that were enriched in *Ms4a4b, Ms4a6b, Dgka, Klf2,* and *S1pr1* exhibited increased frequencies in B6.SAP$^{-/-}$ mice. Just as we observed in neonatal thymic γδ T cells, we noted a near complete loss of mature γδNKT cells (*Zbtb16, Icos*, and *Il4*-enriched γδT2 c8 cells and *Tbx21, Slamf7*, and *Il2rb*-enriched γδT1 c11 cells) as well as a decreased frequency of mature non-γδNKT γδT1 c10 cluster cells in B6.SAP$^{-/-}$ adult thymus (**Suppl. Fig. 8**). Unlike the E17 and neonatal thymic datasets, however, the frequency of γδ T cells with an αβ T cell-like signature in the adult thymic γδ T cell dataset was minimal. Collectively, these data supported the presence of multiple SAP-dependent developmental checkpoints during neonatal and adult γδ T cell development—a reduction in the CD24^{pos}CD73^{neg} SLAMF1^{+}SLAMF6^{+} cluster enriched in γδT17 development-associated transcripts, an increased frequency of immature *S1pr1*-enriched γδ T cells, and decreased frequencies of both γδNKT cells (γδT1 and γδT2) as well as non-γδNKT γδT1 cells.

SAP shapes the thymic γδ TCR repertoire

Given our observation of altered γδ TCR clonotype distribution among E17 γδ T cells and the substantial changes in clustering we observed in SAP-deficient mice, we were next interested in determining the effect of SAP deficiency on the neonatal and adult γδ TCR repertoires. A comparison of frequencies of the top 100 TCR clonotypes between B6 and B6.SAP$^{-/-}$ mice revealed significant changes in the overall frequency of several TRGV1 and TRGV4 clonotypes (**Fig. 5A**). Consistent with a SAP-dependent loss of γδNKT, we observed a profound loss of TRGV1 clonotypes utilizing the canonical TRAV15N-1 and TRAV15-1/TRDV6-1 γδNKT cell TCRs (**Fig. 5B**). Loss of these clonotypes was directly tied to the significant decrease of the γδT1 c8 and γδT2 c13 clusters, in which nearly all these clonotypes resided.

Within the B6 γδT2 c13 cluster the vast majority (~86%) of TCR sequences were highly restricted canonical γδNKT cell clonotypes **(Suppl. Table 2**) and nearly all of these clonotypes were also present in the γδT1 c8 cluster consistent with the ability of γδNKT cells to produce both IFN-γ and IL-4. In contrast, while the B6 γδT1 c8 cluster contained a large proportion of canonical γδNKT cell clonotypes (~46% of c8 TCRs), it also contained TCRs with a diverse pool of clonotypes that utilized TRGV1 (~70% of c8 TCRs), TRGV4, TRGV5, TRGV6, and TRGV7 that were present only in the c8 γδT1 cluster. Therefore, in neonates, the thymic γδT1 population is a mixture of γδNKT and "non-γδNKT" γδT1 clonotypes, and each of these clonotype pools is SAP-dependent. As noted above, these findings were largely reproduced in the adult thymus where the γδNKT clonotypes associated with the c8 and c11 clusters were virtually absent in B6.SAP$^{-/-}$ mice, and where the diverse pool of γδT1 c10 clonotypes was significantly diminished (**Suppl. Table 2)**.

Interestingly, a closer examination of the neonatal thymic TRGV4 clonotypes revealed a significant decrease in the frequencies of γδT17-associated clonotypes with a germline-encoded TRDV5[52] (**Fig. 5B**), some of which were identical to those that were redistributed to the αβ T cell-like c6 cluster in E17 γδ T cells (**Fig. 2E**). When these clonotypes were mapped to their D9 clusters, we noted a significant decrease in the frequency of TRGV4/TRDV5 clonotypes in the mature γδT17 c6 cluster (**Fig 5C**). We note that while we observed a trend toward an increased frequency of TRGV4/TRDV5 and TRGV4/TRDV2 clonotypes in the *S1pr1*$^{+}$ c4/c5 clusters, analysis of these sequences revealed that they largely exhibited diverse CDR3 rather than the restricted CDR3 observed in the γδT17 c6 cluster (**Suppl. Table 2**). Taken together, these data indicated that the immature embryonic day 17 γδ TCR clonotypes that were redirected to the αβ T cell pathway in B6.SAP$^{-/-}$ mice were underrepresented among the mature B6.SAP$^{-/-}$ neonatal γδ T cells.

Restricted TCR repertoire in innate-like γδT1 as well as γδT17 in the periphery

We previously demonstrated that SAP-deficiency results in a significant impairment in γδ T cell function in the periphery[24]. Specifically, we observed that γδ T cell IL-17 production is impaired in the lungs of young mice, but that this had largely corrected itself as the mouse reached maturity. In contrast, we observed that both Vγ1 and Vγ4 IFN-γ production were significantly impaired in B6.SAP$^{-/-}$ adult lung and spleen. To better understand how SAP-dependent alterations in thymic development ultimately affected the peripheral γδ T cell compartment, we compared B6 and B6.SAP$^{-/-}$ lungs using single-cell RNAseq with V(D)J profiling.

Our initial annotation of the B6 lung γδ T cell transcriptome revealed the presence of 11 clusters of the lung γδ T cells that we annotated based on cluster-specific gene expression and TRGV and TRDV usage (**Figure 6A**). Based on their expression of signature cytokines and transcription factors, we identified 2 γδT17 clusters (c1 and c4), 4 γδT1 clusters (c2, c3, c7, and c9), 1 γδTNKT-like cluster (c10) with very few cells, as well as a *Cd24*-enriched cluster (c5) (**Fig. 6B and 6C, Suppl. Table 5**). Consistent with previous observations, we noted that the c1 and c4 γδT17 clusters were enriched in *Slamf1* and that the c2/c3/c7/c9 γδT1 clusters were enriched in *Slamf7* and *Slamf6*

Our initial annotation of the B6 lung γδ T cell transcriptome revealed the presence of 11 clusters of the lung γδ T cells that we annotated based on cluster-specific gene expression and TRGV and TRDV usage (**Figure 6A**). Based on their expression of signature cytokines and transcription factors, we identified 2 γδT17 clusters (c1 and c4), 4 γδT1 clusters (c2, c3, c7, and c9), 1 γδTNKT-like cluster (c10) with very few cells, as well as a *Cd24*-enriched cluster (c5) (**Fig. 6B and 6C, Suppl. Table 5**). Consistent with previous observations, we noted that the c1 and c4 γδT17 clusters were enriched in *Slamf1* and that the c2/c3/c7/c9 γδT1 clusters were enriched in *Slamf7* and *Slamf6* (**Fig. 6B**). Indeed, flow cytometric analysis revealed that SLAMF7 expression was restricted to the innate-like lung $CD44^+CD45RB^+$ γδT1 cell population, and that γδT1 cells are $SLAMF1^-F6^+F7^+$, while the $CD44^+CD45RB^-$ γδT17 subsets are $SLAMF1^+F6^-F7^-$ (**Fig. 6D**). Further annotation using V(D)J profiling revealed that the c1 cluster corresponded to Vγ4 γδT17 (primarily TRGV4/TRDV5 and TRGV4/TRDV2-2) while the c4 cluster corresponded to lung Vγ6 (TRGV6/TRDV4) (**Fig. 6E, Suppl. Table 6**). The c10 cluster was enriched in *Zbtb16*, *Il4*, and *Icos* (**Fig. 6B-C**) as well as TRGV1/TRAV15N-1 and TRGV1/TRDV6 sequences (**Fig. 6E**, **Suppl. Table 6**) consistent with γδNKT cells. We did note, however, that the TRAV15N-1 and TRDV6 sequences in the c10 cluster were, for the most part, non-canonical γδNKT cell clonotypes, suggesting a degree of flexibility in the TRAV15N-1 and TRDV6 CDR3 sequences that can be utilized by γδNKT cells.

Interestingly, while the γδT1 c2/c3/c7/c9 clusters contained primarily Vγ1 and Vγ4 T cells as expected, we noted that Vγ4 γδT1 cells exhibited a striking preference in the usage of TRAV13-4(DV7), and that TRGV4/TRDV7 pairings accounted for 80% of all Vγ4 clonotypes in the γδT1 clusters (**Fig. 6E, Suppl. Table 6**). Analysis of the γδT1 TRAV13-4/DV7 CDR3 sequences revealed a high level of diversity that showed no evidence of clonal expansions (**Fig. 6F**). This was in contrast to the highly restricted Vγ6 repertoire in the c4 γδT17 cluster, as well as the restricted Vγ4 repertoire in the c2 γδT17 cluster that was dominated by semi-invariant TRDV5 and TRDV2-2 sequences (**Fig. 6F**). As no Vδ7-specific antibody was available, we independently confirmed this observation using single-cell PCR to assess the lung Vγ4 CDR3δ sequences from 13 individual mice. These data demonstrated that, other than TRDV2-2 and TRDV5, TRDV7 is the only other TCR delta chain used at an appreciable frequency by Vγ4 T cells in the B6 mouse lung and that it exhibits significant diversity in its CDR3 (**Suppl. Fig. 9**). Vγ1 γδT1 cells, in contrast, exhibited a more mild pairing preference where 44% of the γδT1 clonotypes utilized TRAV15N-1, TRAV15-1/DV6-1, or TRAV15D-2/DV6D-2 and 13% utilized TRAV13-4/DV7 (**Suppl. Table 6**). Together these data formed a comprehensive map of B6 lung γδ T cell transcriptomes and revealed that lung innate-like γδT1, like γδT17 and γδNKT, are all characterized by preferential TCR γ- and δ-chain pairings. This was especially notable for Vγ4 and our data suggested that Vγ4 γδT1 exhibited a distinct preference for the utilization of TRAV13-4(DV7) chains with diverse CDR3.

SAP regulates peripheral Vγ4/Vδ7 γδT1 cells and shapes the lung γδT17 repertoire

Next, we assessed the effect of SAP deficiency on the lung γδ TCR repertoire by comparing B6 and $B6.SAP^{-/-}$ lung γδ T cells (**Fig. 7A**). Consistent with our previous observation that lung γδ T cell IFN-γ production is deficient in SAP-deficient mice[24], we observed a decrease in the frequency of the γδT1 c2, c3, and c7 clusters (**Fig. 7B**). Moreover, we observed a striking decrease in the frequency of TRGV4/TRDV7-expressing cells in the lungs of $B6.SAP^{-/-}$ mice (**Figs. 7C-D, Suppl. Table 6)**, and we noted that we found no evidence of a compensatory increase in the frequency of other TRDV-expressing lung Vγ4 γδT1 cells in the $B6.SAP^{-/-}$ lung. We independently confirmed this SAP-dependent decrease in TRAV13-4/TRDV7 in both lung and spleen using qPCR (**Suppl. Fig. 10**), and we demonstrated a significant decrease in the number of $CD44^+SLAMF7^+$ Vγ4 T cells in both the lungs and spleen of $B6.SAP^{-/-}$ mice (**Fig. 7E**, **Suppl. Fig. 10**). The decreased lung γδT1 did not appear to be due to a SAP-dependent decrease in homeostatic proliferation, nor to increased apoptosis, since we observed no significant change in lung γδ T cell BrdU incorporation or Annexin V staining in $B6.SAP^{-/-}$ mice (**Suppl. Fig. 10**).

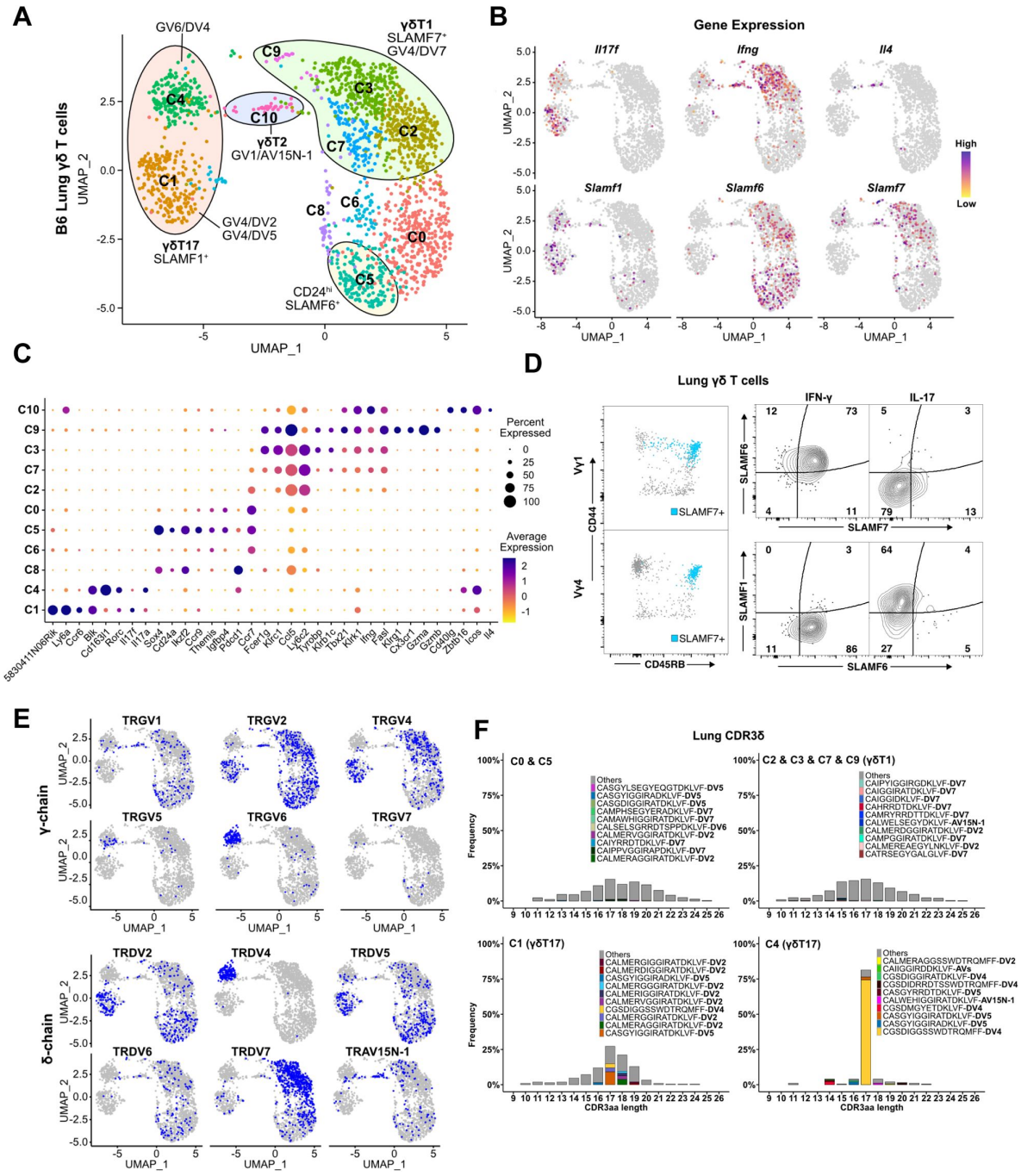

Figure 6.

Restricted TCR repertoire in innate-like γδT1 as well as γδT17 in the periphery.

(A) UMAP representation of B6 adult lung γδ T cells. Clusters are annotated based on gene expression and TCR profiling data. **(B)** Feature plot displaying gene expression profiles of selected genes among individual B6 lung γδ T cells, color-coded based on gene expression levels. **(C)** Dot plot indicating scaled expression levels of selected genes in B6 lung γδ T cells, with dot size representing the fraction of cells within each cluster expressing the marker. **(D)** SLAMF6 and SLAMF7 co-expression marks $CD44^{+}CD45RB^{+}$ IFN-γ-producing cells in the periphery. Representative dot plots (left) of CD44 and CD45RB expression on lung Vγ1 (top) and Vγ4 (bottom) γδ T cells. SLAMF7-expressing cells are highlighted in blue. Representative contour plots (right) of SLAMF1, SLAMF6, and SLAMF7 expression on IFN-$γ^{+}$ and IL-17^{+} lung γδ T cells. **(E)** UMAP representation of B6 lung γδ T cells indicating selected TRG and TRD chain V-segment usage (blue). **(F)** Amino acid length distribution of lung CDR3δ clonotypes among immature C0/C5, γδT1 C2/C3/C7/C9, γδT17 C1, and γδT17 C4 clusters. The top 10 clonotypes in each group are color-coded, while all other clonotypes are shown in gray.

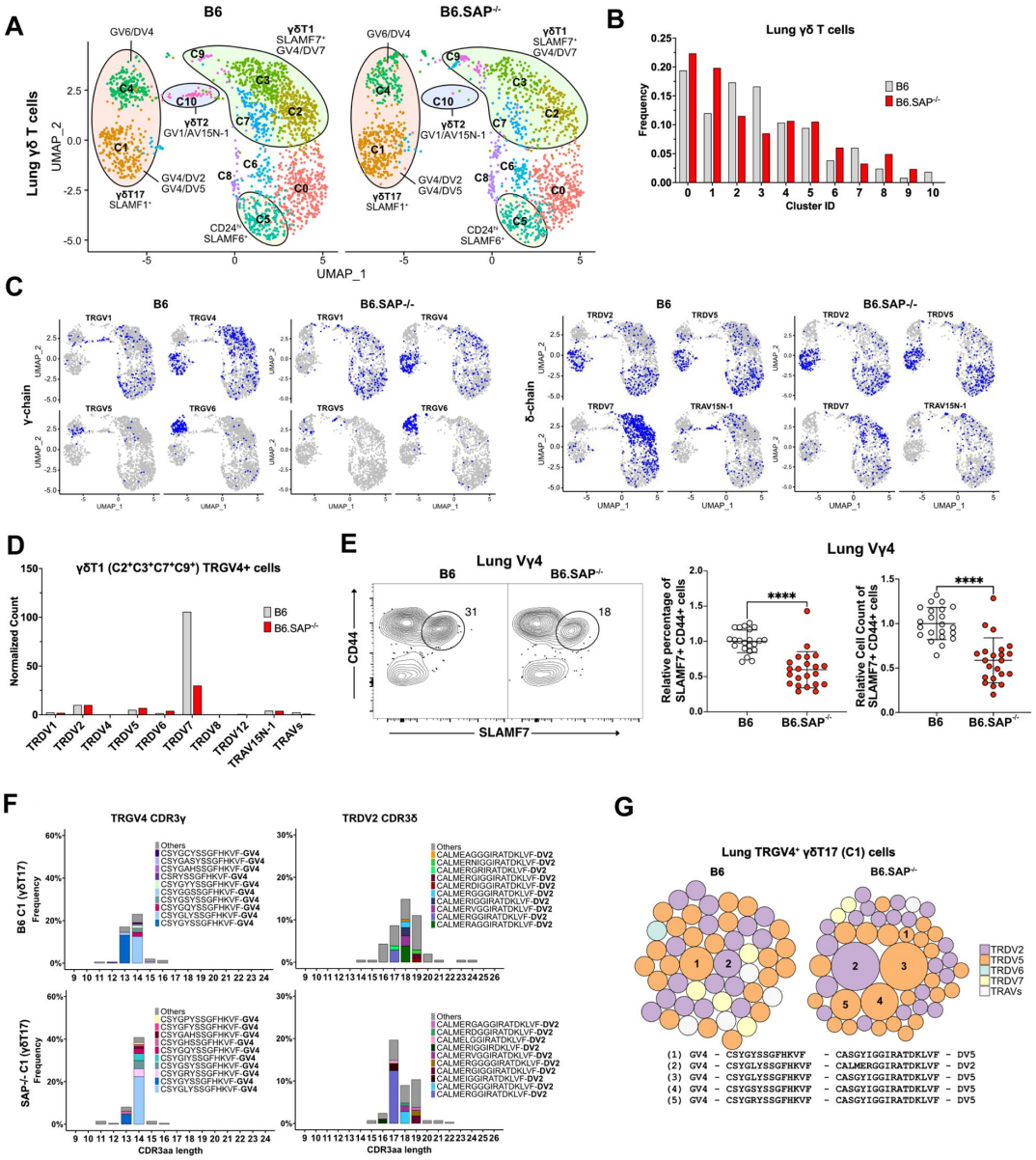

Figure 7.

Specific decrease in Vγ4/Vδ7 γδT1 cells in the lungs of SAP-deficient mice. (A)

UMAP representation of B6 (left) and B6.SAP$^{-/-}$ (right) lung γδ T cells, pooled from 3 mice per strain. **(B)** SAP-dependent variation in lung γδ T cell cluster frequencies. The frequency of each B6 and B6.SAP$^{-/-}$ cluster as a percentage of all lung γδ T cells is shown. (**C**) UMAP representation of selected TRG and TRD chain V-segment usage (blue) among B6 and B6.SAP$^{-/-}$ lung γδ T cells. **(D)** SAP-dependent decrease in lung γδT1 TRGV4/TRDV7. Normalized TRDV counts in B6 and B6.SAP$^{-/-}$ lung TRGV4^{+} γδT1 clusters (C2/C3/C7/C9). **(E)** SAP-dependent decrease in SLAMF7^{+} lung Vγ4 T cells. Representative contour plots of CD44 and SLAMF7 expression in B6 (left) and B6.SAP$^{-/-}$ (right) lung Vγ4 γδ T cells are shown at *left*. Relative frequencies and counts of CD44^{+}SLAMF7^{+} lung Vγ4 cells is shown at *right*. Data represent the cumulative data from five independent experiments, ****p < 0.0001 using unpaired t-test. **(F)** SAP-dependent skewing of the lung γδT17 TCR repertoire. Amino acid length distributions of B6 and B6.SAP$^{-/-}$ TRGV4^{+} CDR3γ (left) and TRDV2^{+} CDR3δ (right) sequences in the lung Vγ4 γδT17 C1 cluster. The top 10 clonotypes are color-coded and all other clonotypes are shown in gray. Bars represent the frequency of γδ T cells in the c1 cluster. **(G)** TCR clonotype bubble plots depicting the top 50 lung TRGV4 clonotypes in the C1 γδT17 cluster. Bubble size indicates clonotype frequency as a percentage of C1 Vγ4 (n = 62 B6, 104 B6.SAP$^{-/-}$) T cells, and colors correspond to specific TRDV chains. Selected clonotypes are numbered and their corresponding CDR3γ and CDR3δ sequences are displayed below.

In addition to the decrease in lung γδT1, we also noted a loss of the c10 γδT2 cluster consistent with the enrichment in SAP-dependent γδNKT TCRs in this cluster, and we observed an increased frequency of the Vγ4 γδT17 c1 cluster (**Fig. 7B**). Given our previous observation of a SAP-dependent decrease in lung γδ T cell IL-17 production in young, but not adult mice[24], and our findings here of SAP-dependent alterations in γδT17 clonotypes, we were interested in determining whether the adult lung γδT17 repertoire was altered in SAP-deficient mice. Indeed, a comparison of the lung Vγ4 c1 γδT17 CDR3 sequences between B6 and B6.SAP$^{-/-}$ mice revealed significant alterations in the γδT17 c1 cluster TCR repertoire. Specifically, we noted a decreased frequency of TRGV4 chains that exhibited a germline-encoded CDR3γ (CSYGYSS) and an increased frequency of TRGV4 chains with a CDR3γ exhibiting evidence of N/P additions (CSYG(X)YSS). These changes were associated with a significant shift in the usage of TRDV2-2 CDR3δ sequence usage (**Fig. 7F**) and an altered c1 TCR clonotype frequency in B6.SAP$^{-/-}$ mice (**Fig. 7G**). Although the number of germline-encoded invariant TRGV4/TRDV5 clone (clonotype 1 in **Fig. 6B**) was diminished in B6.SAP$^{-/-}$ lung γδ T cells (**Fig. 7G**, **Suppl. Table 6**), the low numbers of cells available for analysis precluded us from making strong conclusions regarding the loss of any one particular clonotype. Taken together, these data suggest that Vγ4 γδT1 preferentially utilize the TRAV13-4(DV7) chain in the lung and that the SAP-dependent decrease in peripheral γδ T cell IFN-γ production is not due to dysregulated cytokine production, but rather due to a specific loss of innate-like γδT1 subsets. This finding, together with our finding that the adult lung γδT17 TCR repertoire is altered in SAP-deficient mice suggests that SLAM/SAP signaling plays a role in shaping the γδ TCR repertoire.

Discussion

A common denominator in most innate-like T cell developmental programming is a dependence on the SLAM/SAP signaling pathway[17, 24, 25, 61]. Within the γδ T cell lineage, SAP plays a critical role in the development of IFN-γ and IL-4-producing γδNKT cells[27], as well as in γδT1 and γδT17[24], but exactly when during γδ T cell development SAP functions, and how it exerts these effects is unknown. Here, we provide evidence that SAP mediates its effects on immature, uncommitted thymic γδ T cells and that it works to simultaneously promote progression through the γδT17 developmental pathway while inhibiting the diversion of γδ T cells into the αβ T cell pathway. The redirection of γδ T cell clonotypes into the αβ T cell pathway at E17 is associated with a decreased frequency of these mature clonotypes in neonatal thymus, and an altered γδT17 TCR repertoire in the periphery. Finally, we identify Vγ4/Vδ7 T cells as a novel, SAP-dependent IFN-γ-producing Vγ4 γδT1 subset.

The developmental pathway(s) that gives rise to γδ T cell functional subsets remains unclear. γδ T cells develop at the DN2/DN3 stage after receiving a sufficiently strong γδTCR-mediated signal[62]. Numerous reports support a model where, within the continuum of signals that can drive γδ T cell development, it is the relatively weaker TCR signals that promote γδT17 programming while the stronger TCR signals foster γδNKT and γδT1 programming[4, 14, 17, 20, 63, 64]. Despite considerable effort, the precise thymic developmental stages at which γδ T cell lineage diversification occurs remains unclear. Recent studies examining this issue have demonstrated that effector programming can occur at a CD44^{neg}CD45RB^{neg} stage[4, 20], and that c-Maf-directed γδT17 programming occurs at a CD45RB^{low} stage[42]. In addition, by altering TCR signal strength in a transgenic model, Chen et al., defined a *Ccr9*-enriched cluster as a point of effector lineage diversification[16]. Our findings here suggest that SAP influences γδT17 developmental programming during the immature uncommitted CD24^{hi}CD73^{neg} stage, either during or soon after *Il2ra (*CD25) downregulation. The SAP-dependent c2 cluster we define here was highly enriched in numerous genes (e.g., *Sox13*[46], *Blk*[41], *Maf*[42], *Etv5*[45], *Sh2d1a*[24]) previously associated with γδT17 development as well as *Ccr9*, and the cell surface phenotype of c2 γδ T cells is SLAMF1^{pos}SLAMF6^{pos}CD44$^{low/high}$CD45RB^{low}. Altogether, these data suggest that the SAP-dependent c2 cluster is identical to these previously defined developmental checkpoints. Given

that these previous studies have demonstrated that this developmental checkpoint is influenced by TCR signaling, it is interesting to note that SLAM/SAP signaling has previously been demonstrated to foster semi-invariant NKT cell differentiation through its ability to regulate TCR signal strength[65].

To that end, we noted that the SAP-dependent c2 cluster in E.17 γδ T cells was enriched in *Blk*, *Lck*, and *Fyn*, Src tyrosine kinase family members that have all been implicated in γδ T cell development[41, 60]. Decreased expression of *Blk*, which is known to promote γδT17 development[41], in B6.SAP$^{-/-}$ γδ T cells suggests one possible mechanism through which SAP may regulate γδT17 development via TCR signaling. The mechanism, however, through which SAP regulates *Blk* gene expression remains unclear. Since SAP is known to regulate conventional αβ T cell signaling through its ability to recruit FYN[66, 67] and LCK[68, 69] to SLAM family members, it seems reasonable to hypothesize that SAP could regulate TCR signaling by recruiting one or more of these Src kinase family members to the γδ TCR signalosome.

Our finding that SAP inhibited the number of γδ T cells that enter the αβ T cell developmental pathway is reminiscent of previous work using transgenic TCR models demonstrating that a reduction of TCR signal strength results in a redirection of γδ T cells to the αβ T cell lineage[59, 70]. Fahl et al. recently demonstrated that both entry into the γδ T cell lineage as well as γδ T cell effector programming involved repression of TCF1 expression by TCR-driven increases in *Id3*[48]. Consistent with these results, we found that *Tcf7* (encoding TCF1) transcript levels were highest in the αβ T cell-like c6 cluster, and we note that *Tcf7* transcripts levels were noticeably higher in the *Il2ra*-enriched post-selection c5 cluster in B6.SAP$^{-/-}$ γδ T cells. *Id3* expression, however, did not appear to be appreciably altered in SAP-deficient mice. Whether SAP-mediated signals could alter γδ T cell *Tcf7* expression through a TCR-independent mechanism remains an open question.

In addition to the considerable evidence supporting a role for TCR signal strength in γδ T cell developmental programming, there is increasing support for a model in which γδT17 programming occurs earlier in development, prior to expression of the γδ TCR. Indeed, evidence that some DN1 thymocytes possess a SOX13^{hi} IL-17-like phenotype and that Vγ4 γδT17 arise from DN1 precursors[18, 71] indicates the existence of such a TCR-independent developmental programming stage. In consideration of such a model, it may be possible that SLAM/SAP-mediated signals could differentially regulate the survival and/or fitness of the functionally pre-programmed γδ T cell subsets. Such a function would be consistent with the role of SLAMF6 and SAP in promoting reactivation-induced cell death in conventional αβ T cells[69, 72].

While our data indicate that SAP regulates the diversion of at least some TCR clonotypes into the αβ TCR pathway, the fate of those cells is unclear. Certainly, the fact that the clonotypes that were diverted to the αβ T cell pathway in E17 thymus are under-represented in the mature D9 thymus γδT17 clusters suggests that this diversion has significant consequences on the γδ T cell receptor repertoire, but whether these diverted γδ T cells contribute to the αβ T cell compartment is unclear. Recently, a population of hybrid αβ-γδ T cells was described in both mouse and human[73] that responds to peptide/MHC stimulation like conventional αβ T cells, as well as to IL-1 and IL-23 which induce both IFN-γ and IL-17 production[73]. In the mouse, at least some of these cells are Vγ4/Vδ5, Vγ4/Vδ4, or Vγ4Vδ7 and are present in the embryonic thymus, raising the possibility that γδ T cells diverted to the αβ T cell pathway in B6.SAP$^{-/-}$ mice contribute to this αβ-γδ T cell population. While we have not observed a significant increase in the overall numbers of αβ-γδ T cells in B6.SAP$^{-/-}$ thymus (not shown), a direct comparison of B6 and B6.SAP$^{-/-}$ αβ-γδ TCRs may be necessary to see such an effect.

Our previous observations that SAP deletion did not completely abolish the development of IL-17- and IFN-γ producing γδ T cells[24] suggested the possibility that SAP may be critical for the development of additional γδ T cell clonotypes other than the Vγ1Vδ6.3 subset. Therefore, we compared the SAP-dependent and SAP-independent γδTCR repertoires using paired TCR clonotype

analysis, which allowed us to track clonotype fate during development. Our findings not only confirmed previous results demonstrating highly restricted γδT17[51], [52], and γδNKT[27] TCR repertoires, they also revealed that the vast majority of Vγ4 γδT1 subsets in the periphery preferentially utilize TRGV4/TRAV13-4(DV7) clonotypes, thereby further highlighting the strong links between γδ T cell function and the utilization of specific TCRs[29]. The reason for this preferential TRDV usage in Vγ4/Vδ7 γδT1 is unclear. While the TRAV13-4(DV7) CDR3 sequences were diverse and did not suggest evidence of clonal expansion, it may be possible that TRDV-encoded sequence motifs could be required to interact with a ligand, similar to the way that TRGV-encoded sequences mediate recognition of butyrophilins[74], [75].

Exactly when during development SAP exerts its effects on Vγ4/Vδ7 T cells is still somewhat unclear. We found comparatively low numbers of TRGV4/TRDV7 γδ T cells in embryonic, neonatal, or adult thymus, and those that were identified were generally found in the immature clusters. The increased frequency in B6.SAP$^{-/-}$ E17 thymus of TRGV4/TRDV7 γδ T cells in the *Il2ra*$^{+}$ c5 cluster coupled with their decreased frequency in the emigrating *S1pr1*$^{+}$ c4 cluster suggests a model where SAP promotes progression through the early stages of development through thymic egress. SAP deficiency, therefore, could result in lower Vγ4/Vδ7 output. However, this model is at odds with our finding that the frequency of *S1pr1*$^{+}$ clusters in neonatal thymus is increased in B6.SAP$^{-/-}$, and that these clusters contained increased numbers of TRGV4/TRDV7 γδ T cells. A possible explanation could be found in a previous report demonstrating that a Vγ4/Vδ7 subset increases in frequency in the periphery of B6 mice over time and undergoes extrathymic expansion[76]. Our finding here that that the Vγ4/Vδ7 T cells represent a SAP-dependent innate-like γδT1 subset raise the possibility that SAP regulates the homeostatic expansion of this subset after it leaves the thymus. The mechanism, however, through which SAP is regulating the number of Vγ4/Vδ7 T cells remains unclear, as we have so far observed no evidence of changes in homeostatic proliferation or apoptosis of these cells in the lungs.

We previously demonstrated that the SAP-dependent impairment in γδT17 function in the neonatal periphery largely corrects itself as mice mature[24]. This suggested the possibility that SAP-dependent γδT17 clonotypes originating in the embryonic thymus were being replaced over time by SAP-independent γδT17 clonotypes. Although our data certainly point to a SAP-dependent decrease in a germline-encoded Vγ4/Vδ5 clonotype in neonatal thymus, the low numbers of this clonotype in the lung makes it difficult to draw definitive conclusions in the periphery. Still, we did observe a role for SAP in shaping the peripheral γδT17 repertoire, as we noted a decreased frequency of germline-encoded TRGV4 sequences (so-called "GYSS"[77]) coupled with an increased frequency of TRGV4 sequences with more diverse CDR3 ("GXYSS") in the periphery. Although the potential significance of this change on γδ T cell function is unclear, it does support a model in which SAP regulates γδT17 developmental programming during embryonic thymic development, where the low expression of terminal deoxynucleotide transferase results in a high frequency of germline-encoded V-J junctions.

In summary, our findings reveal the presence of multiple SAP-dependent developmental checkpoint during the very early stages of γδ T cell development in the thymus, indicating a more complex role for this signaling pathway in γδ T cell developmental programming than previously appreciated. Indeed, our data indicate that SAP functions to regulate entry into the γδ and αβ T cell developmental pathways, and we make the striking observation that nearly all Vγ4 γδT1 cells in the periphery preferentially use Vδ7 chains and that it is a decrease in the Vγ4/Vδ7 subset that, in part, underlies the SAP-dependent decrease in γδ T cell IFN-γ production. Altogether, these findings suggest that SAP regulates the balance of innate-like γδT1/γδT2/γδT17 subsets during thymic development and in the periphery.

Methods

Mice

C57BL/6J (B6) and B6.*Sh2d1a*$^{-/-}$ (SAP$^{-/-}$) mice were purchased from the Jackson Laboratory (Bar Harbor, ME) and were housed and bred in a specific pathogen-free facility at the animal facility of the University of Vermont. For experiments using E17 mice, timed-pregnant matings were used. The presence of a vaginal plug indicated day 0 of pregnancy. The flow cytometry experiments included 8-13 weeks old B6 and B6.SAP$^{-/-}$ mice (age and sex-matched). All experimental procedures on animals were carried out with the approval of the University of Vermont Institutional Animal Care and Use Committee.

Tissue Processing

Single-cell suspensions from the spleen and thymus were obtained by gently passing tissue through nylon mesh. Red blood cells (RBCs) were lysed with Gey's solution. Single-cell suspensions from the lungs were prepared as described (Benoit et al., 2015). Briefly, dissected lungs were finely minced in a digestion buffer containing DMEM, 1 mg/ml collagenase type IV (Gibco), and 0.2 mg/ml DNase (Sigma-Aldrich). After shaking at 200 rpm at 37°C for 20 min, the lung digests were triturated with a 16-gauge needle, followed by an additional 20 min shaking at 200 rpm at 37°C. Following the final trituration, red blood cells (RBC) were lysed with Gey's solution. Finally, the digested lung tissues were filtered through a 70-µm filter and washed in PBS/2%FBS. Cells were counted either on a MACSQuant VYB or using a hemacytometer following trypan blue staining.

Flow Cytometry

Cells were incubated with LIVE/DEAD™ Fixable Blue Dead Cell stain (Thermo Fisher Scientific, Grand Island, NY) for 30 min at 4°C in PBS, after which they were resuspended in Fc-Block (BioLegend) containing PBS/2% FCS/0.1% sodium azide buffer. After a 5-10 min incubation on ice, antibodies specific for cell surface markers were added, incubated for 30 min on ice, and washed in PBS/2% FCS/0.1% sodium azide buffer. Brilliant Violet Staining buffer (BD Biosciences) was used in experiments contain more than one Brilliant Violet, Brilliant UV, or SuperBright-conjugated Ab. Cells were fixed in PBS/1% PFA buffer and stored at 4° C prior to data collection.

For nuclear staining, cells were permeabilized with Foxp3 transcription factor fixation/permeabilization buffer (ThermoFisher) following surface staining. Cells were incubated overnight at 4°C, washed, and incubated with 25 micrograms/ml total rat IgG before adding Abs against transcription factors. After staining, cells were washed and resuspended in PBS/2% FCS/0.1% sodium azide buffer. For intracellular cytokine staining, cells were permeabilized with PBS/1% FCS/0.1% sodium azide/0.1% saponin following surface staining and fixation. To reduce unspecific binding, 25 µg/ml total rat IgG was added prior to cytokine staining with fluorescent-labeled antibodies.

Flow cytometry data were collected on a Cytek® Aurora (Cytek Biosciences) spectral cytometer, and data analysis was performed using FlowJo Software (Tree Star). In some cases, visualization of flow cytometry data was conducted by concatenation of individual .fcs files, followed by dimensionality reduction and clustering using UMAP and FlowSOM[78] in FlowJo. Antibodies used in these experiments are anti-CD4 (RM4-5), anti-CD11b (M1/70), anti-CD11c (N418), anti-CD19 (1D3), anti-CD24 (M1/69), anti-CD25 (PC61), anti-CD27 (LG.3A10), anti-CD44 (IM7), anti-CD45RB (C363-16A), anti-CD73 (TY/11.8), anti-CD150 (TC15-12F12.2), anti-CD196 (29-2L17), anti-CD319 (4G2), anti-cMAF (sym0F1), anti-IFNγ (XMG1.2), anti-IL17a (TC11-18H10.1), anti-IL4 (11B11), anti-PLZF (9E12), anti-T-bet (4B10), anti-TCRβ (H57-597), anti-Vγ5 (536), and anti-Vd6.3 (C504.17c) from BioLegend; and anti-RORγt (Q31-378), anti-TCRδ (GL3), anti-Vγ1 (2.11) from BD biosciences; and anti-CD8a (53-

6.7), anti-CD45 (30-F11), anti-CD200 (OX90), anti-CD278 (7E17G9), anti-Ki-67 (SolA15), anti-Ly108(13G3-19D), anti-Vγ4 (UC3-10A6) from eBiosciences; anti-S1P1 (713412) from R&D systems; anti-Blk (polyclonal) from Cell Signaling Technology; and anti-17D1

In vivo proliferation and apoptosis

For *in vivo* proliferation analysis, each mouse was intraperitoneally injected with 1 mg of 5-bromo-deoxyuridine (BrdU) (Sigma-Aldrich) each day for 3 days. Lung cell suspensions were prepared as above, stained with surface markers, after which they staining with anti-BrdU antibody according to the manufacturer's instructions (BrdU Flow Kit; BD Biosciences). For apoptotic cell detection, annexin V staining was performed. Briefly, surface staining was followed by dead cell staining with Fixable Viability Dye eFluor™ 780 dye. The cells were washed and resuspended in an annexin-binding buffer (10 mM HEPES, 140 mM NaCl, and 2.5 mM CaCl2, pH 7.4). Finally, 1 µl of Annexin V Conjugate (Thermo Fisher Scientific, Grand Island, NY) was added to each tube, and cells were incubated for 15 minutes at room temperature (RT) prior to data collection.

Bulk RNA Sequencing and data analysis

For the bulk RNA sequencing, thymocytes from 10-day old B6 (n=4 male, n=2 female) and B6.SAP$^{-/-}$ (n=5 male, n=1 female) mice were prepared by depleting CD4+ cells from thymocytes using the EasySepTM Mouse CD4 Positive Selection Kit II (STEMCELL Technologies). Cells were then incubated with Fixable Viability Dye eFluor™ 780 (Thermo Fisher Scientific, Grand Island, NY) for 30 min at 4°C in PBS, after which they were resuspended in Fc-Block (BioLegend) containing PBS/2% FCS. After washing, cells were stained with antibodies against CD11b (M1/70), CD19 (1D3), CD24 (M1/67), CD45 (30-F11), TCRβ (H57-597), and TCRδ (GL3) for 30 min at 4°C. Following surface staining, CD24^{hi}TCRδ+ cells were sorted from a CD11b^{-}CD19^{-}TCRb-population of live CD45^{+} lymphocytes. Immature (CD24^{high}) thymocytes from both B6 and B6.SAP$^{-/-}$ mice were sorted directly into 350 microliters of RLT lysis buffer (Qiagen). RNA was extracted using the RNeasy Micro kit (Qiagen) according to manufacturer instructions. After RNA quantification and quality assessment, cDNA libraries were prepared using SMARTer Stranded Total RNA-Seq Kit v3 - Pico Input Mammalian (Takara, Japan) according to the manufacturer's protocol. Following library clean-up and quantification, the libraries were sequenced (single-end 75 bp) on an Illumina HiSeq1500.

The Fastq files were checked for data quality using FastQC and MultiQC[79] bioinformatics tools. Cutadapt[80] was used to filter out low-quality sequences and to remove adapter sequences from all reads. The expression of transcripts was quantified using the mapping-based mode of Salmon[81], which quasi-mapped RNA-seq reads to an index created from a mouse reference transcriptome (GRCm39). The transcript abundance estimates were imported using tximport[82] and differential gene expression (DE) analysis was performed using DEseq2[83] employing the Wald test of the negative binomial model coefficients to determine statistical significance. The results were analyzed based on Log_2 fold change ($Log_2FC \geq 0.5$ or ≤ -0.5) and adjusted P-value (padj ≤ 0.0001) to determine whether a gene was differentially expressed.

Cell sorting and library preparation for CITE-seq and V(D)J enrichment

For thymus single-cell transcriptome analysis, we used embryonic day 17 (E17) B6 (n=4) and B6.*Sh2d1a*$^{-/-}$ (SAP$^{-/-}$) (n=4) mice, nine day-old (D9) B6 (n=3) and B6.SAP$^{-/-}$ (n=3) mice, and six-week-old B6 (n=3 male) and B6.SAP$^{-/-}$ (n=2 male, n=1 female) mice. For single-cell analysis of adult lung γδ T cells, we used 13 week old B6 and B6.SAP$^{-/-}$ littermates (pooled cells from 2 males and one female mouse in each group).

Analysis of gene expression, surface protein expression, and TCR V(D)J repertoire was performed using the 10X Genomics Chromium Next GEM Single Cell 5' V(D)J with feature barcoding kit (version 1.1). To sort cells for scRNAseq, thymocytes were stained with anti-TCRδ-PE (GL3) antibody and enriched using anti-PE MicroBeads kit (Miltenyi Biotec). The exception was E17 thymus which did not undergo TCRδ enrichment. Following live/dead staining with Fixable Viability Dye eFluor™ 780 (Thermo Fisher Scientific, Grand Island, NY) for 30 min at 4° C in PBS, cells were resuspended in Fc-Block (BioLegend) containing PBS/2% FCS. Cells were then simultaneously stained with oligonucleotide-conjugated antibodies targeting CD24, CD44, CD45RB, CD73, SLAMF1, SLAMF6, Vγ1, and Vγ4 (TotalSeqC-BioLegend), oligonucleotide-conjugated hashtag antibodies (TotalSeqC-BioLegend), and fluorophore-conjugated antibodies for cell sorting which included the anti-CD11b (M1/70), anti-CD11c (N418), anti-CD19 (1D3), anti-CD45.2 (104) and anti-TCRβ (H57-597) antibodies. Following surface staining of the enriched population, $TCR\delta^+$ cells were sorted from a $CD11b^-CD11c^-CD19^-TCR\beta^-$ population of $CD45.2^+$ live lymphocytes.

Libraries were prepared according to the manufacturer's instructions with modifications to the V(D)J enrichment procedure. Equal numbers of live $GL3^+$ γδ T cells from B6 and $B6.SAP^{-/-}$ mice were pooled and captured (between 5000 – 7000 cells) using a 10x Chromium controller. Following cDNA preparation, the gene expression and CSP libraries were created according to the manufacturer's instructions. To obtain TCR gamma and delta chain sequences, we replaced kit-provided enrichment primers with custom mouse γ and δ chain-specific primers and modified the number of PCR cycles used from manufacturer recommended cycling conditions. In the first enrichment step, an equal amount of cDNA was used as a template for PCR amplification of γ and δ chains separately using a total of 12 and 10 PCR cycles, respectively. The primers used for the first γ-chain enrichment are: Forward Primer 5'-AATGAT ACGGCGA CCACCG AG ATCTACACTCTT TCCCTACAC GACGCTC-3' (2 μM) and Reverse Outer Primers 5'-GGAA AGAACTT TTCAAGGAS ACAAAG-3' (1 μM), 5'-CCCTTATG ACTTCAGG AAAGAA CTTT-3' (0.5 μM). The primers used for the first δ-chain enrichment are: Forward Primer 5'-AATGAT ACGGCGACCACCG AGATCTACACTC TTTCCCTAC ACGACGCTC-3' (2 μM) and Reverse Outer Primer 5'-CCACAATC TTCTTGGATG ATCTGAG-3' (0.5 μM). Following PCR product purification, the γ-chain and δ-chain amplicons went through the second round of enrichment separately using a total of 12 and 10 PCR cycles, respectively. The primers used for the second γ-chain enrichment are: Forward Primer 5'-AATGA TACGGCGACCA CCGAGATCT-3' (0.5 μM) and Reverse Inner Primers 5'-ACAAA GGTATGTCCCA GTCTTATGGA-3' (0.5 μM), 5'-GGAGACA AAGGTAGGT CCCAGC-3' (0.5 μM). The primers used for the second δ-chain enrichment are: Forward Primer 5'-AATGATA CGGCGACCACC GAGATCT-3' (0.5 μM) and Reverse Inner Primer 5'-GTCACCTC TTTAGGGTAG AAATCTT-3'. Following PCR product cleanup, the second round PCR products (γ-chain and δ-chain amplicons) were quantified and combined in equal quantity making the final TCR V(D)J library. Finally, all three libraries (gene expression, cell surface protein expression, and TCR V(D)J) were sequenced (paired-end 26 x 91 bp) on an Illumina HiSeq 1500 sequencer or a NextSeq 2000.

CITE-seq quality control, filtering and demultiplexing

Raw sequence reads from the gene expression and CSP libraries were processed using the Cell Ranger software (v4.0.0)[84]. Reads were mapped to the GRCm38 (mm10) mouse reference genome. To exclude the possibility of TCR transcripts playing a role in UMAP clustering, all TCR genes were omitted from the analysis using the "cellranger reanalyze" argument of Cell Ranger software.

Quality control, filtering, UMAP projection, and clustering analysis were conducted using Seurat (v4.3.0.1)[85] R package. Briefly, cells with a low number (≤2000 for E17 thymus dataset, ≤1200 for D9 thymus dataset and ≤750 for lung dataset) of unique genes (nFeature_RNA), a frequency of mitochondrial reads > 4% and a frequency of ribosomal protein < than ~12% were eliminated from further analysis. To reduce cell cycle-related and stress-related heterogeneity in the normalized data, selected cell cycle genes and stress-induced genes [86] were regressed out during the data normalization step. Note that in some instances, contaminating clusters expressing

macrophage specific marker genes were manually removed using Seurat "CellSelector ()" argument. We used the Seurat function "HTODemux()" to demultiplex single cells back to their sample of origin [87].

CITE-Seq and V(D)J enrichment data analysis

The demultiplexed datasets were further analyzed for gene expression, cell surface protein expression following the multimodal analysis pipeline of Seurat[85]. For each dataset, we performed normalization and variance stabilization of the gene expression data using the scTransform[88]. Following identification of top significant principal components (PCs) using the principal component analysis (PCA), we performed a graph-based (UMAP) semi-supervised clustering of cells with similar gene expression patterns using specific number of top PCs (E17 = 25, D9 = 30, W6 = 27, lung = 28) and resolution values (E17 = 1.2, D9 = 1.6, W6 = 0.65, lung =1.2) for each dataset. The cell surface protein expression data (Centered Log Ratio (CLR) normalized) from CSP libraries as well as the gene expression data were then visualized on the clustered cells using the R package scCustomize[89]. The differentially expressed features of each cluster (cluster biomarkers) were identified using FindAllMarkers() function using the Wilcoxon Rank Sum test. For identifying differentially expressed genes (DEGs) between B6 and B6.SAP$^{-/-}$ samples, we performed a pseudobulk DE (differential expression) analysis of aggregated read counts using the DEseq2 package, which accounts for biological replicates making it a better approach than other specialized single-cell DE analysis methods[90]. Briefly, for cells of a given sample type, we aggregated RNAseq reads across biological replicates identified by individual hashtags. Then transformed the genes-by-cell matrix to a genes-by-replicates matrix and performed DE analysis using the DESeq2[83] package employing the Wald test of the negative binomial model coefficients to determine statistical significance. Finally, the trajectory and pseudotime inference analysis was performed using the partition-based graph abstraction (PAGA)[91] analysis, which is a part of the Scanpy[92] python package.

For the analysis of V(D)J library sequences, Cell Ranger v6.1.2 ("cellranger vdj" argument) was used to map the TCR V(D)J) reads to a custom-made reference containing sequences from the IMGT database[93]. The Cell Ranger V(D)J output was then processed with custom bashscripts. Briefly, the TRGV and TRAV/TRDV contigs identified by Cell Ranger V(D)J were demultiplexed to individual barcodes after which the dominant TRGV and TRAV/DV transcripts were selected per cell. Finally, the V(D)J information of each cell was integrated with scCITE-seq data and visualized using a combination of Seurat and custom-made R scripts. We note that since about half of Vγ1, Vγ4, and Vγ7 T cells contain functionally rearranged TRGV2 chains, but only a small percentage express Vγ2 on the cell surface[94], the methods used here cannot adequately assess the true TRGV2 repertoire. Therefore, we report it here for accuracy but have omitted TRGV2 from our analysis.

Quantitative PCR

Lung qPCR samples were prepared by positively selecting leukocytes using CD45 MicroBeads (Miltenyi Biotec). Spleen qPCR samples were prepared by depletion of CD19+ TCRβ+ cells using biotinylated antibodies and Streptavidin MicroBeads (Miltenyi Biotec) according to the manufacturer's instructions. Total RNA was extracted from approximately 5-10 million cells from each organ using the RNeasy Mini Kit (QIAGEN). SuperScript® IV Reverse Transcriptase (Thermo Fisher Scientific, Grand Island, NY) was used to generate cDNA using 400 ng of RNA and oligodT primer according to the manufacturer's instructions. qPCR was performed using 1µl of cDNA template in iTaq Universal SYBR Green Supermix (Bio-Rad) containing TCR delta chain specific primer pairs. The qPCR reaction was run on a Bio-Rad CFX96 qPCR machine using the following cycling conditions: 95°C for 30 sec; 40 cycles of [95°C for 5 sec; 60°C for 30 sec; 72°C for 30 sec]. The β2M and TRDC genes were used as endogenous housekeeping controls. Primers used were as follows: mb2mforward, 5'-CATGGCTCG CTCGGTGACC-3', mb2mreverse, 5'-AATGTGAGGC GGGTGGAACTG-3', TRDCforward, 5'-CTCCGGCCA AACCATCTGTT-3', mouseDV2, 5'-CCAAGAAG

CATACAAGCAGT ATAATG-3', mouseDV5, 5'-CCCATGA TGCAGATTT TGTTCAAGG-3', mouseDV7, 5'-GGAAG MCTCGTCAGC CTGTTGT-3', mouseDCrev, 5'-CCACAATCTT CTTGGAT GATCTGAG-3'. Some primer sequences were adopted from Wei. et. al. (2015)[51].

Vγ4 single cell sorting and TCR Sequencing

The plate-based based γδ TCR repertoire analysis of single-cell sorted Vγ4 cells involved adult lungs from 8-10 weeks old B6 male (n=7) and female mice (n=6). Lung Vγ4 TCR sequences were obtained using a protocol modified from Wei *et al.*, (2015)[51]. Briefly, lung cell suspensions were prepared as described above. After washing, cells were resuspended in Fc-Block (BioLegend) containing PBS/2% FCS buffer, and stained with anti-CD11b (M1/70), anti-CD11c (N418), anti-CD19 (1D3), anti-CD45 (30-F11), anti-TCRδ (GL3) and anti-Vγ4 (UC3-10A6) from for 30 min at 4°C in PBS. Fixable Viability Dye eFluor™ 780 (Thermo Fisher Scientific, Grand Island, NY) was used to identify dead cells. Single-cell sorting of lung $V\gamma4^{+}TCR\delta^{+}$ from a $CD11b^{-}$ $CD11c^{-}CD19^{-}TCR\beta^{-}$ population of $CD45^{+}$ live lymphocytes were performed using a FACS Aria III cell sorter (BD Bioscience). Cells were sorted directly into 12.5 µl (per well) of OneStep RT-PCR Buffer mix (QIAGEN) in a 96-well PCR plate (one cell/well).

TCR sequences were then amplified and barcoded according to (Wei *et al.*, 2015). Briefly, the first two nested PCR reactions involved primer-specific amplification of gamma and delta TCR sequences. In both the first and second PCR reactions, the final concentration of each V-region primer is 0.36µM, and each C-region primer is 0.6µM. The first RT-PCR step was performed using the following cycling conditions: 50°C for 30 min; 95°C for 5 min; 25 cycles of [94°C for 30 sec; 62°C for 1min; 72°C for1 min]; 72°C for 7 min; 4°C. Next, 1 µl of the first round PCR product was used as a template for the second nested PCR reaction using HotStartTaq Master Mix Kit (QIAGEN). The cycling conditions for the second PCR reaction were 95°C for 5 min; 25 cycles of [94°C for 30 sec; 64°C for 1min; 72°C for1 min]; 72°C for 7 min; 4°C. In the third PCR reaction, 1 µl of second round PCR product as the template in a new 14 µl reaction using HotStartTaq Master Mix Kit (QIAGEN). Each well was barcoded. The final concentration of 5' and 3' barcoding primers was 0.05µM each and paired-end primers were 0.5µM each. The cycling conditions for the third PCR reaction were 95°C for 5 min; 36 cycles of [94°C for 30 sec; 62°C for 1min; 72°C for1 min]; 72°C for 7 min; 4°C. The γ and δ chain products were run on 1.2% agarose gel separately and purified using the Qiagen QIAquick Gel Extraction Kit according to kit instructions. The final products were then analyzed using the 2100 Bioanalyzer (Agilent Technologies). Finally, the γ and δ TCR products were mixed in equal concentration and sequenced on the Illumina MiSeq platform using the Illumina MiSeq Reagent Kit v2 (500-cycles).

The paired-end TCR sequencing reads were analyzed using a custom software pipeline capable of de-multiplexing barcoded sequences to individual cells. The resulting de-multiplexed reads were then analyzed by MiGMAP software, which identifies CDR3 sequences using the IgBlast 1.4.0 (NCBI) V(D)J mapping tool[95, 96]. The single-cell TCR V(D)J profiling data were then visualized using custom R scripts.

Statistical analysis

Prism (GraphPad Software, San Diego, CA) was used for the statistical analysis of data. Unpaired Student t-tests, one-way ANOVA, or two-way ANOVA were used where appropriate. Tests were considered significant when p-values were less than 0.05. Error bars represent standard deviation (SD) unless otherwise indicated.

Acknowledgements

We thank Marlana Winschel, Cameron Moquin, and Erin Mathieu for help in tissue preparation and flow cytometry. We acknowledge Roxana del Rio Guerra for help in cell sorting. All flow cytometry data were collected at the Harry Hood Bassett Flow Cytometry and Cell Sorting Facility (Larner College of Medicine, University of Vermont) and was supported by NIH grant (S10OD026843). We thank Jessica Hoffman, Kris Finstaad, and the Vermont Integrated Genome Resource (Larner College of Medicine, University of Vermont) for help in scRNAseq, Julie Dragon and Korin Eckstrom for help in bioinformatics analysis. We thank Fred Kolling at the Genomics Shared Resource (Dartmouth Geisel School of Medicine) for help in sequencing. We also thank Willi Born and Rebecca O'Brien for the 17D1 hybridoma and Pablo Pereira for helpful discussion. This work benefitted from data assembled by the ImmGen consortium, and was supported by NIH grants R21AIO66465 and R03AI153902, S10OD026843 (JEB) and an AAI Careers in Immunology Fellowship (SKM, JEB).

Author contributions

S.K.M. and J.E.B. conceived and designed the project; S.K.M., J.E.B., E.A., K.J.H., B.M.H., R.S., and O.D. performed experiments and analyzed data; K.J.H., D.G., J.T.R., and N.S. aided with the single-cell TCR sequencing; D.M. assisted with bulk RNA sequencing; S.K.M. and J.E.B. performed the bioinformatics analysis of bulk RNA-seq and single-cell CITEseq (with immune profiling) data; J.E.B. supervised the project; S.K.M. and J.E.B. prepared the manuscript.

Data Availability

All sequencing data in this manuscript have been deposited in NCBI GEO and have been assigned the accession number GSE262064. All scripts used in these analyses have been made publicly available on Github and can be accessed here: *https://github.com/Boyson-Lab/scRNAseq_with_immune_profiling_tutorial*

Competing interests

All authors declare no competing interests.

Supplementary Figure Legends

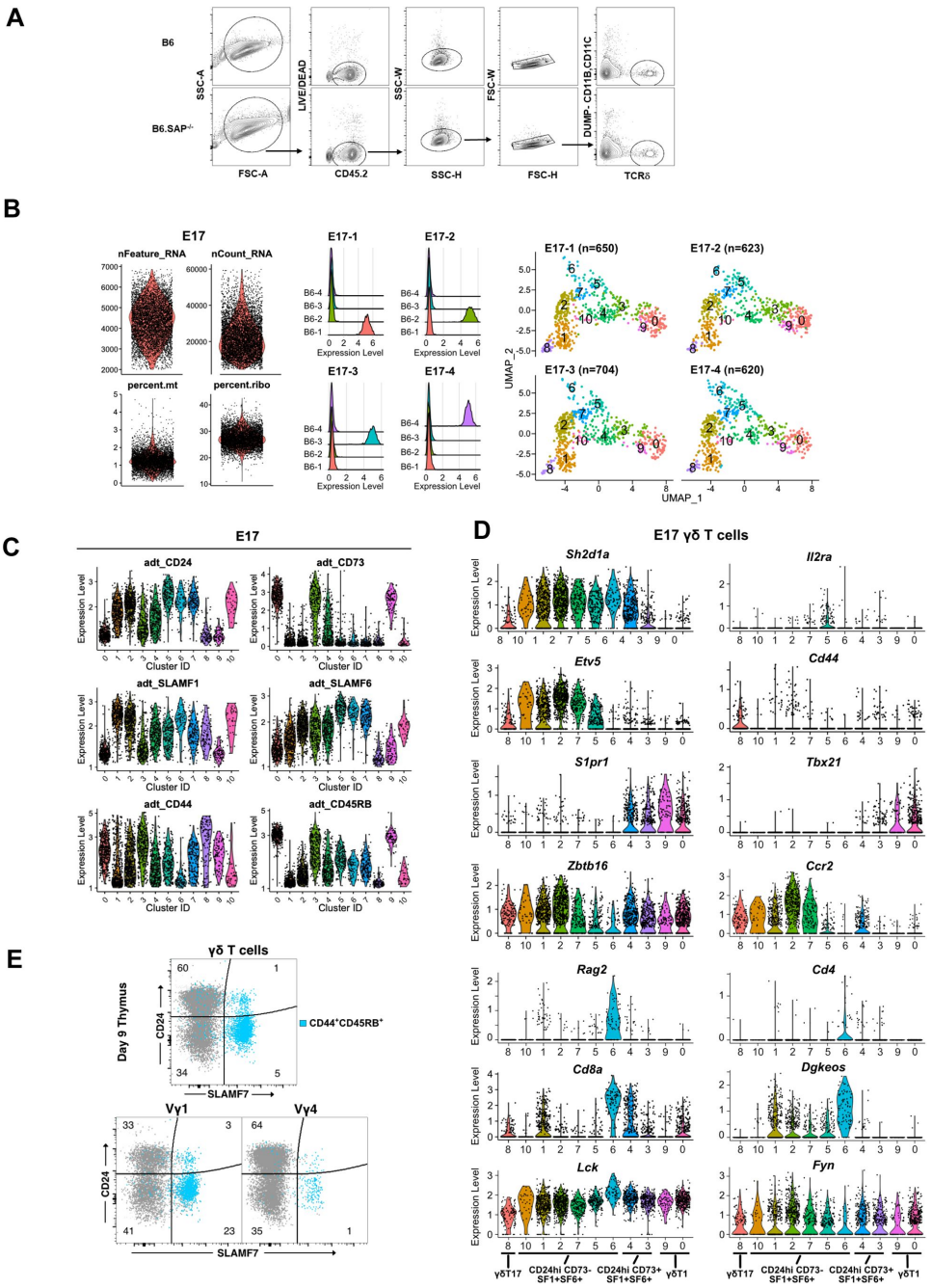

Supplemental Figure 1

Quality control for single cell CITE-seq.

(A) Representative gating scheme used for FACS sorting γδ cells from B6 (top) and B6.SAP$^{-/-}$ (bottom) thymus. **(B)** *Left,* Violin plots of B6 E17 thymic γδ T cells. nFeaure_RNA represents number of genes detected in each cell. nCount_RNA represents total number of molecules detected within a cell, percent.mt represents the frequency of mitochondrial genes expressed in each cell, and percent.ribo represents the frequency of ribosomal genes expressed in each cell. *Middle,* ridge plots demonstrating successful enrichment for selected hashtags in E17 thymus γδ T cells following demultiplexing. *Right,* UMAP representations showing distribution of demultiplexed γδ T cells among individual B6 E17 thymus samples. **(C)** Violin plots depicting distribution of cell surface protein oligo-conjugated antibody derived tags (ADTs) among different B6 E17 thymus γδ T cells clusters. **(D)** Violin plots depicting expression levels of selected genes among individual E17 B6 thymic γδ T cells clusters. **(E)** Representative dot plots of CD24 and SLAMF7 staining on neonatal thymus γδ T cells. The position of CD44^{+}CD45RB^{+} cells are shown in blue. Data are representative of two independent experiments, n = 10 mice.

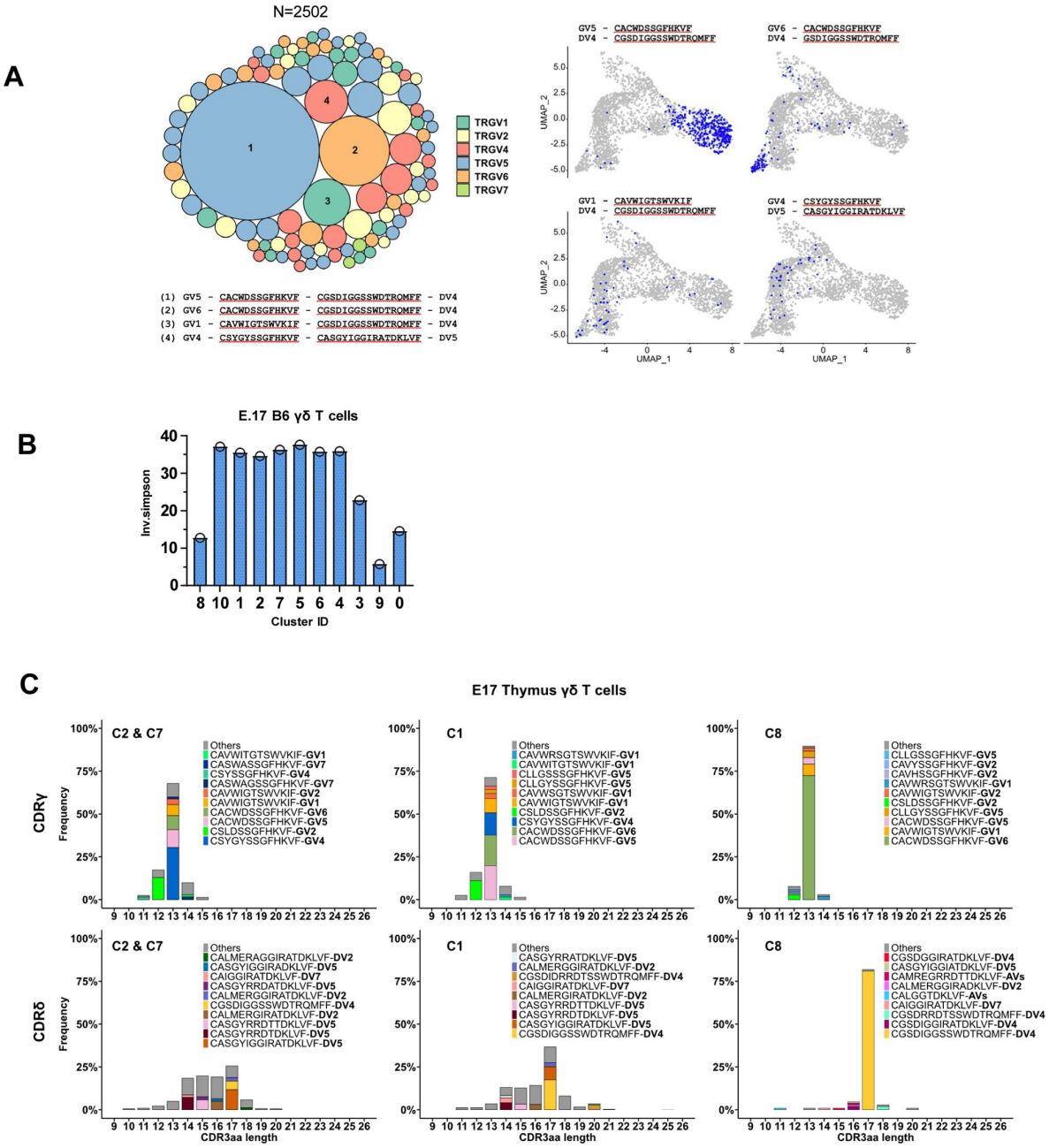

Supplemental Figure 2

TCR repertoire profiling of B6 E17 thymus γδ T cells.

(A) *Left,* TCR clonotype bubble plot depicting the top 100 TCR clonotypes among B6 E17 γδ T cells (n = 2502 γδ T cells). Each bubble represents a unique TRGV/TRDV clonotype; the bubble size corresponds to the clonotype frequency, and colors correspond to specific TRGV chains utilized. The 4 most frequent clonotypes are numbered and their corresponding CDR3γ and CDR3δ sequences are displayed below. *Right*, UMAP representations depicting the location of the four most frequent clonotypes E17 thymic γδ T cell clusters. **(B)** Diversity of the E17 γδ TCR repertoire, represented by the Inverse Simpson index. **(C)** Amino acid length distributions of E17 thymic γδ T cell CDR3γ (top) and CDR3δ (bottom) in immature *Blk*$^{+}$, *Etv5*$^{+}$, *Maf*$^{+}$ C2 and C7 (left), immature RORγt^{high} C1 (middle), and mature RORγt^{high} c8 (right) clusters. The top 10 clonotypes are color-coded, all other clonotypes are shown in gray.

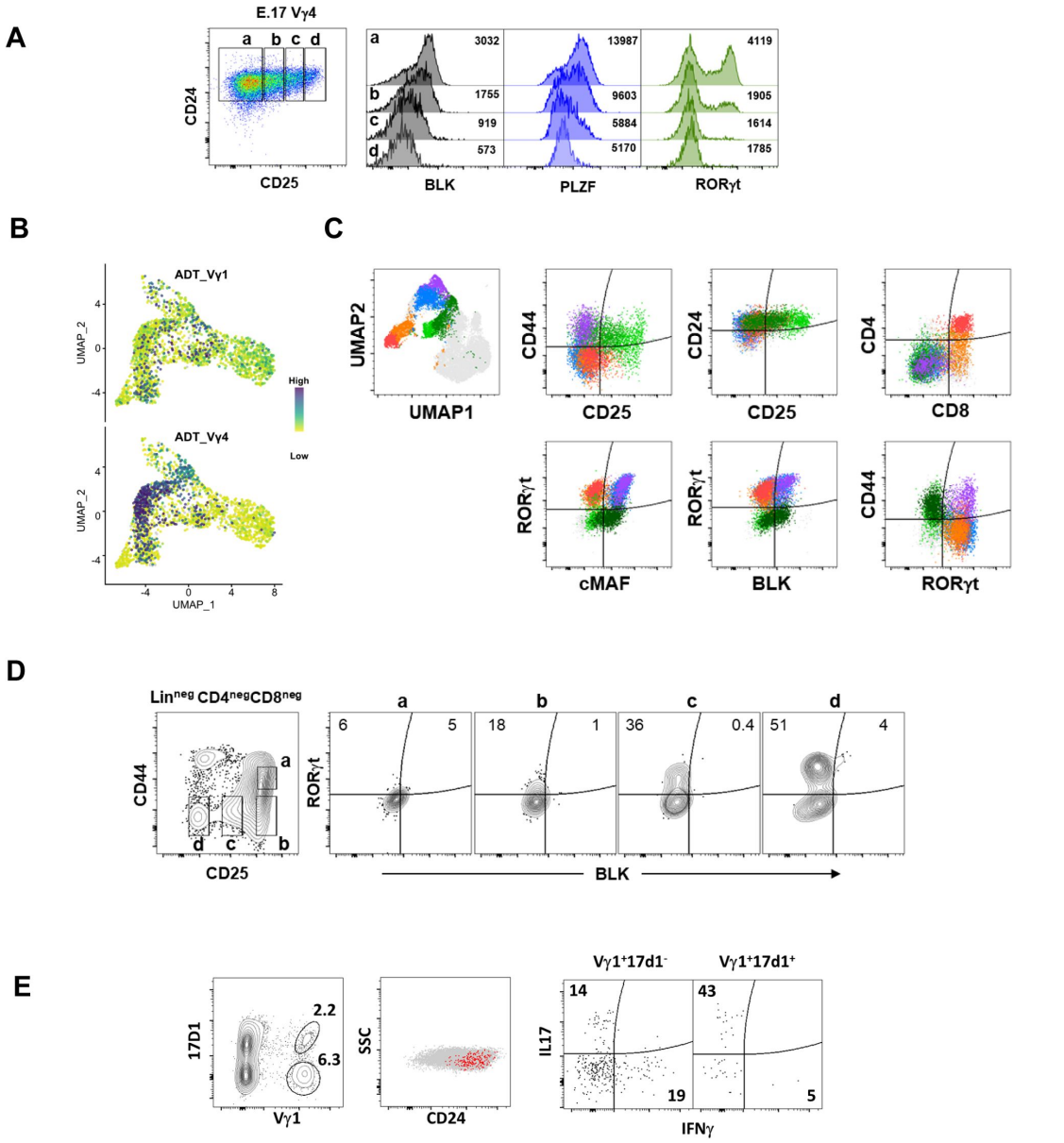

Supplemental Figure 3

Identification of a BLK^{neg}MAF^{neg}RORγt^{pos} E17 γδ T cell population expressing CD4 and CD8.

(A) *Left,* Representative dot plot of CD24 and CD25 expression on E17 B6 thymic Vγ4 T cells. *Right,* Histograms depicting BLK, PLZF, and RORγt expression in the gated populations at left. The geometric mean fluorescence intensity of individual populations is shown. **(B)** Feature plots showing cell surface protein expression of Vγ1 (top) and Vγ4 (bottom) on B6 E17 thymus γδ T cells. Each point represents a cell, color-coded based on the protein expression level (high: dark blue, low: yellow). **(C**) *Top left*, UMAP representation of E17 B6 γδ T cell flow cytometry data with selected FlowSOM clusters indicated by color. All other cells are shown in gray. *Right,* Individual dot plots overlaid with the selected FlowSOM clusters from the UMAP plot. Data represent concatenated data from 5 B6 TCRβ^{neg}TCRδ^{pos} γδ T cells and are representative of 2 independent experiments. **(D)** Increasing BLK^{neg}RORγt^{pos} frequency as thymocytes progress to DN4 stage. Representative contour plots of E17 DN thymocytes with selected gates shown (*left*) and BLK and RORγt expression associated with each gated population (*right*). Numbers indicate the percentage of cells in the gated population. **(E)** Immature Vγ1Vδ1 T cells comprise the major IL17-producing Vγ1 T cell population in E17 thymus. *Left,* representative contour plot of Vγ1 and Vδ1 (17D1) expression among E17 thymic γδ T cells. *Middle,* Dot plot of CD24 and SSC expression on E17 thymic γδ T cells. The position of Vγ1^{+}Vδ1^{+} E17 T cells is shown in red. *Right,* Dot plots of IL-17 and IFN-γ expression in E17 thymic Vγ1^{+}17D1^{+} and Vγ1^{+}17D1^{-} cells after PMA/ionomycin stimulation.

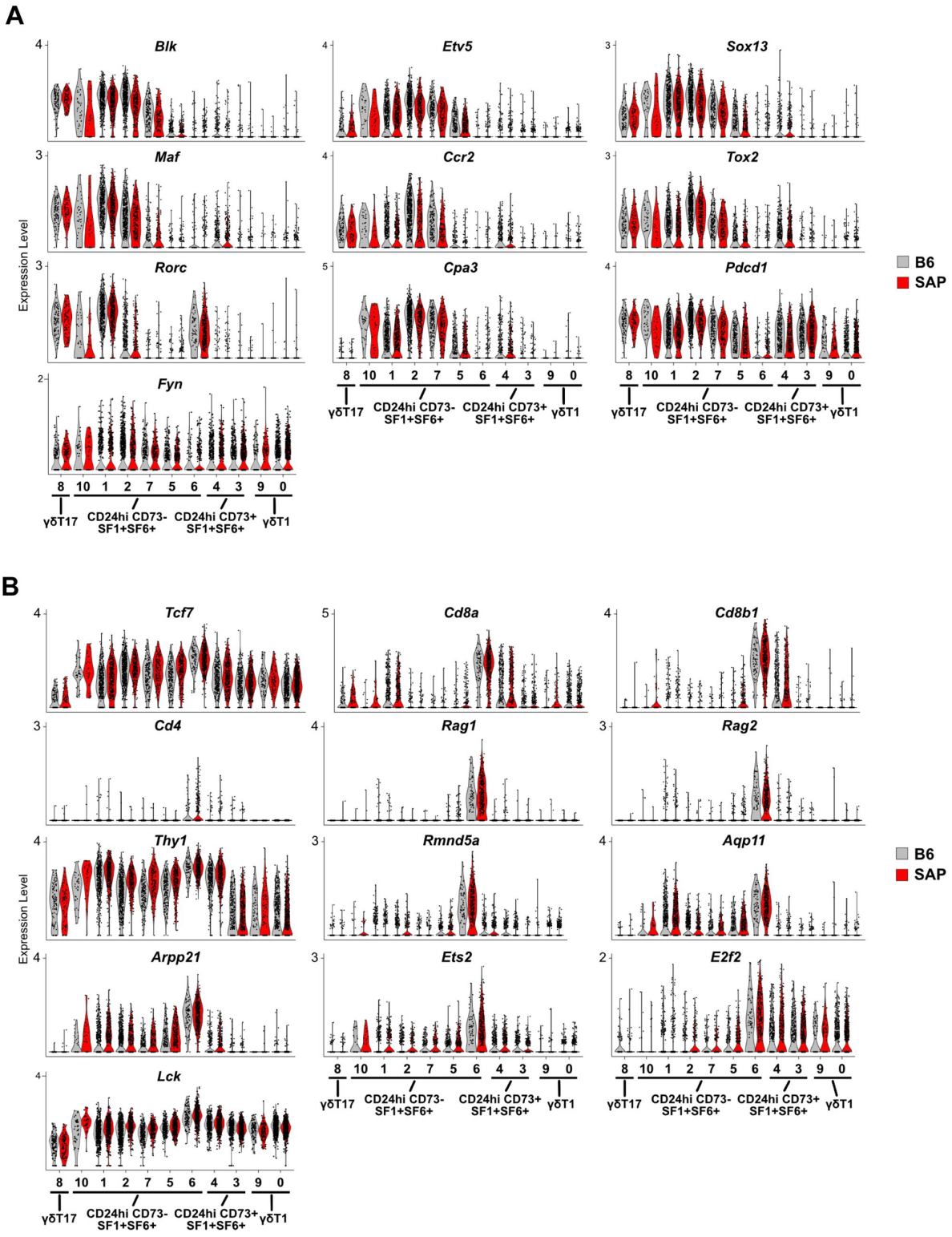

Supplemental Figure 4

Violin plots showing expression levels of selected genes among individual B6 and B6.SAP$^{-/-}$ E17 thymic γδ T cell clusters. **(A)** Genes whose expression decreased in B6.SAP$^{-/-}$ immature γδ T cells. **(B)** Genes whose expression increased in B6.SAP$^{-/-}$ immature γδ T cells.

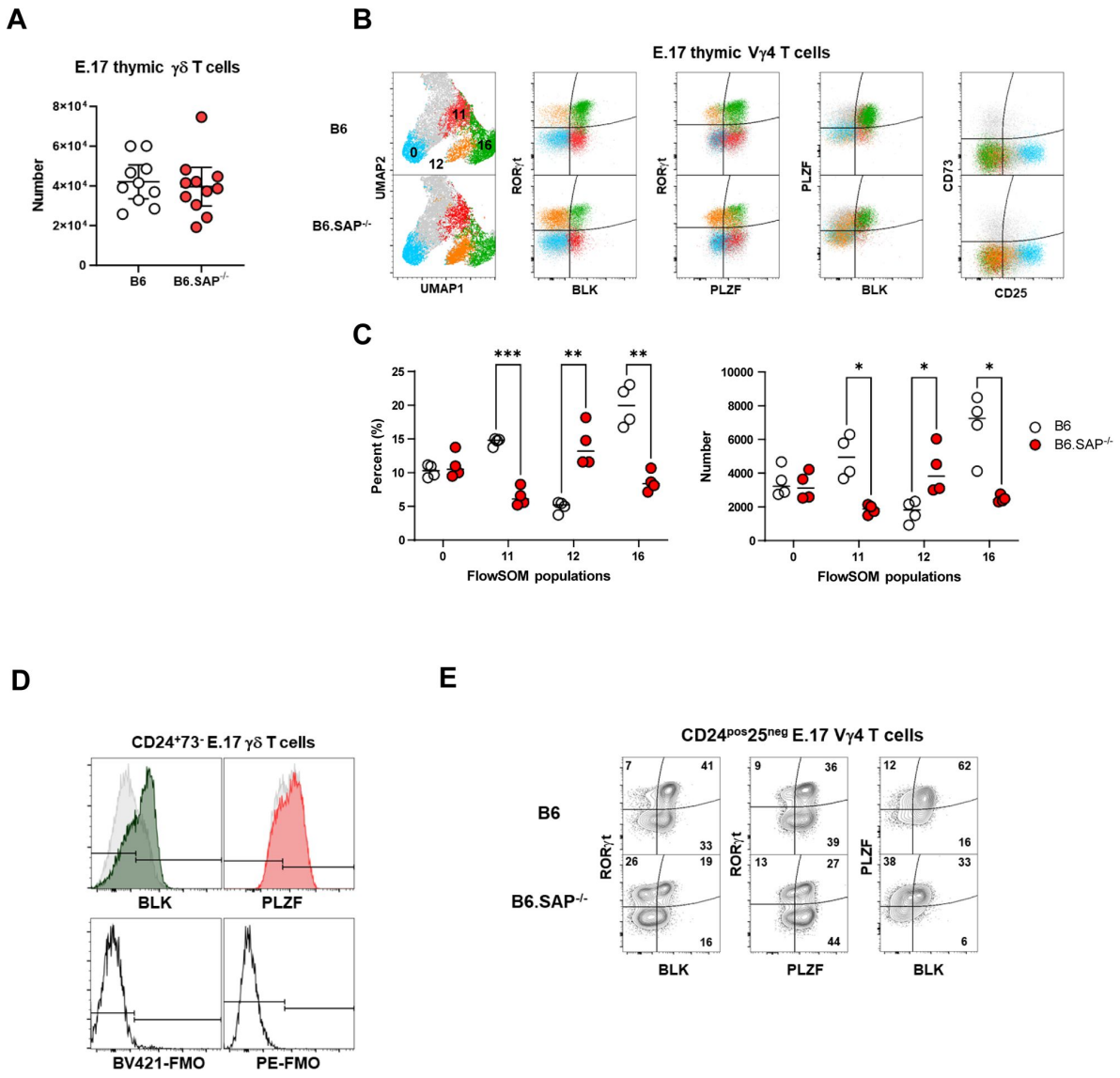

Supplemental Figure 5

SAP-dependent regulation of immature BLK^{+}PLZF^{+}RORγt^{+} and BLK^{-}PLZF$^{+/-}$RORγt^{+} E17 thymic γδ T cells.

(A) Total number of E17 thymic γδ T cells in B6 and B6.SAP$^{-/-}$ E17 thymus. **(B)** E17 thymic Vγ4 developmental checkpoints. *Left, U*MAP representation of E17 B6 and B6.SAP$^{-/-}$ Vγ4 T cell flow cytometry data with selected FlowSOM clusters indicated by color. All other cells are shown in gray. *Right,* Individual dot plots overlaid with the selected FlowSOM clusters from the UMAP plot. Data represent concatenated data from 4 B6 and 4 B6.SAP$^{-/-}$ TCRβ^{neg}TCRδ^{pos} γδ T cells and are representative of 2 independent experiments. **(C)** Cumulative frequency and number of the indicated FlowSOM populations shown in (B), *p ≤ 0.05, **p ≤ 0.01, ***p ≤ 0.001, unpaired t-test, corrected for multiple comparison using Holm-Sidak's test. **(D)** Decreased BLK, but not PLZF expression in B6.SAP$^{-/-}$ γδ T cells. *Above,* histograms of BLK and PLZF in immature E17 γδ T cells. B6 BLK (dark gray) and PLZF (red) histograms are overlaid on B6.SAP$^{-/-}$ (light gray) histograms for comparison. *Below,* control stains lacking BLK or PLZF. **(E)** Representative contour plots of immature CD25^{neg} E.17 Vγ4 T cells in B6 and B6.SAP$^{-/-}$ mice.

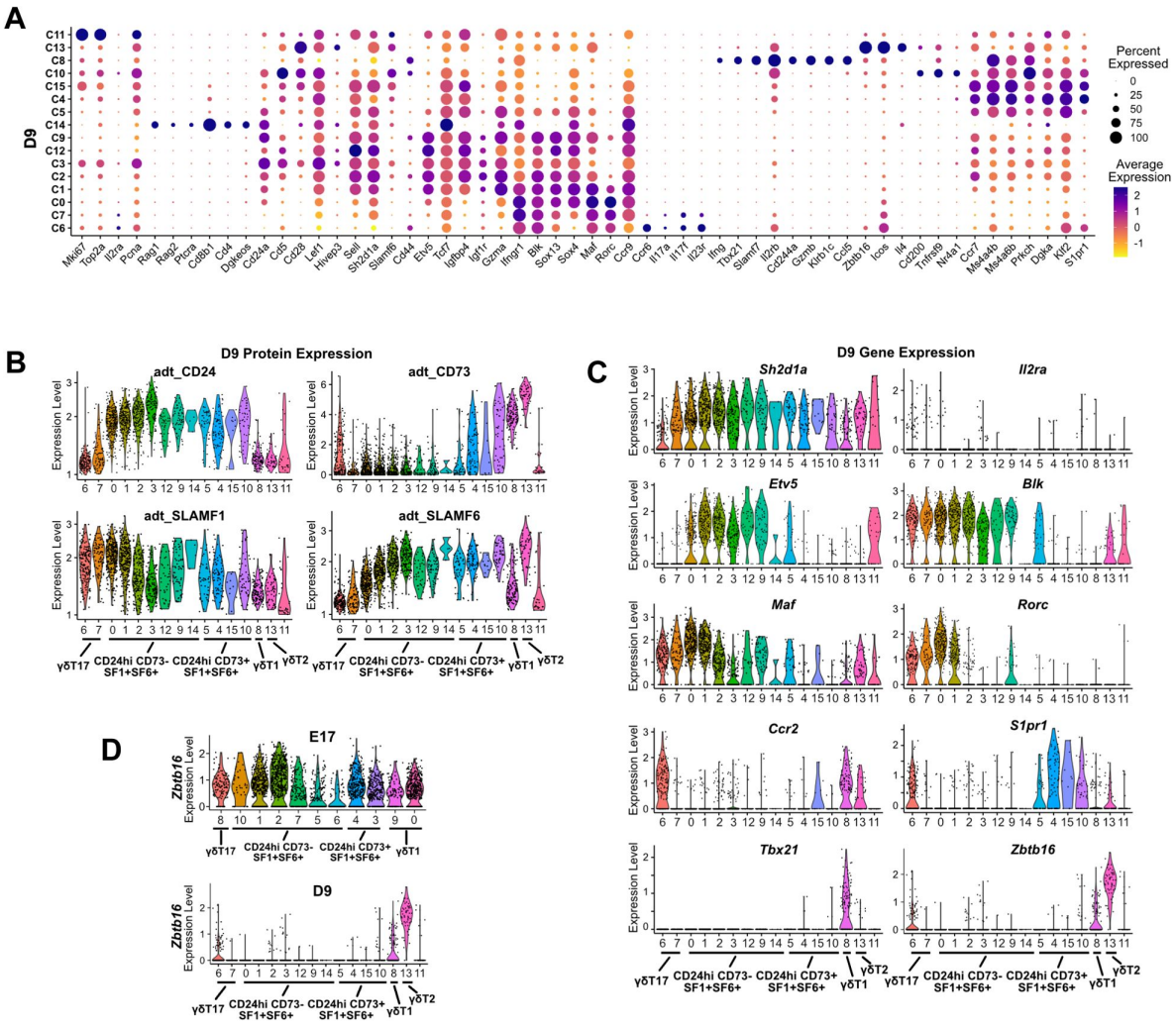

Supplemental Figure 6

Transcriptional heterogeneity in neonatal thymic γδ T cells.

(A) Dot plot showing scaled expression level of selected genes in B6 D9 thymic γδ T cells. Level of normalized expression is shown using a color scale ranging from low (yellow) to high (purple). Dot size represents the fraction of cells within each cluster that express the marker. **(B)** Violin plots showing the specificity of the oligo-conjugated antibody derived tags (ADT) to cell surface proteins (CD24, CD73, SLAMF1, SLAMF6) among different B6 D9 thymus γδ T cell clusters. **(C)** Violin plots showing expression levels of selected genes among individual clusters in the B6 D9 thymic γδ T cells. **(D)** Violin plots showing expression levels of *Zbtb16* gene (expressing PLZF) among individual clusters in the B6 E17 (top) and D9 (bottom) thymic γδ T cells.

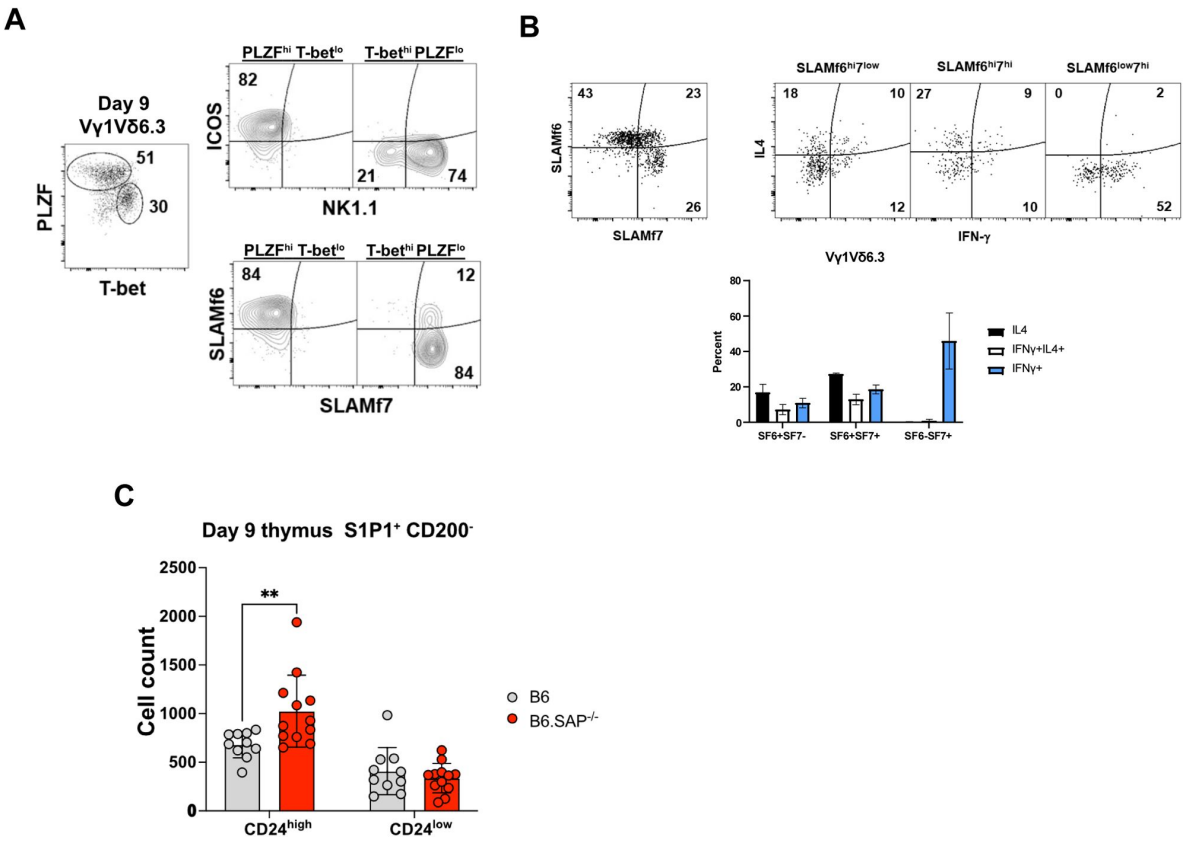

Supplemental Figure 7

Flow cytometric analysis of D9 thymic γδ T cells.

(A) SLAMF6 and SLAMF7 expression defines γδNKT cell subsets. *Left*, representative dot plot of PLZF and T-bet expression in B6 D9 thymic Vγ1Vδ6.3 γδNKT cells. Representative contour plots of ICOS and NK1.1 (*top right)* and SLAMF6 and SLAMF7 (*bottom right*) staining in PLZF^{hi}T-bet^{low} and PLZF^{low}T-bet^{high} subsets are shown at right. Data are representative of two independent experiments with a total of ten mice. **(B)** *Left,* representative dot plot of SLAMF6 and SLAMF7 expression in B6 D9 thymic Vγ1Vδ6.3 γδNKT cells. *Right,* representative dot plots of intracellular IL4 and IFN-γ expression in SLAMF6^{hi}SLAMF7^{low}, SLAMF6^{high}SLAMF7^{hi}, and SLAMF6^{low}SLAMF7^{hi} γδNKT cell subsets. Numbers indicate percentage. Cumulative data of IL-4 and IFN-γ expression is shown below. Data are representative of two independent experiments with a total of ten mice. **(C)** Increased number of immature CD200^{-}S1P1^{+} γδ T cells in SAP-deficient neonatal thymus.

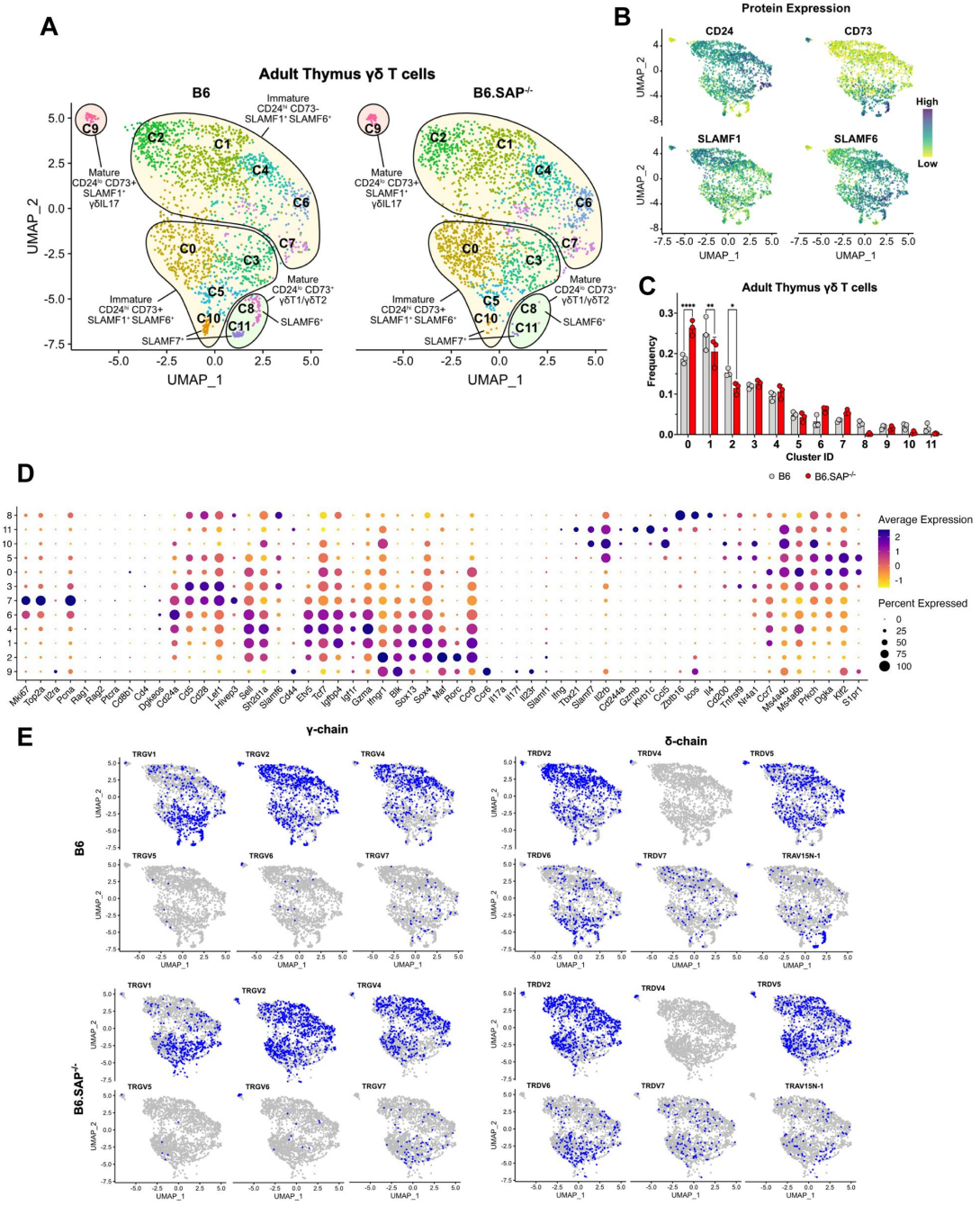

Supplemental Figure 8

scRNA-seq with TCR repertoire profiling of B6 and B6.SAP$^{-/-}$ adult thymic γδ T cells.

(A) UMAP representation of B6 and B6.SAP$^{-/-}$ adult thymus (6 weeks old) γδ T cells, n = 3 mice per strain. **(B)** Feature plots illustrating the cell surface protein expression profiles of CD24, CD73, SLAMF1, and SLAMF6 on adult thymic γδ T cells. Each data point represents a cell, color-coded to indicate varying protein expression levels (high: dark blue, low: yellow). **(C)** Frequencies of B6 and B6.SAP$^{-/-}$ γδ T cell clusters. Bars represent the mean cluster frequency, error bars represent standard deviation, *p ≤ 0.05, **p ≤ 0.01, ****p ≤ 0.0001, two-way ANOVA, Sidak multiple-comparisons test. **(D)** Dot plot showing scaled expression level of selected genes in B6 adult thymic γδ T cells. Level of normalized expression is shown using a color scale ranging from low (yellow) to high (purple). Dot size represents the fraction of cells within each cluster that express the marker. **(E)** Expression of selected TRG (left) and TRDs chain (right) V-segment usage (blue) by individual adult thymus γδ T cells in B6 and B6.SAP$^{-/-}$ mice.

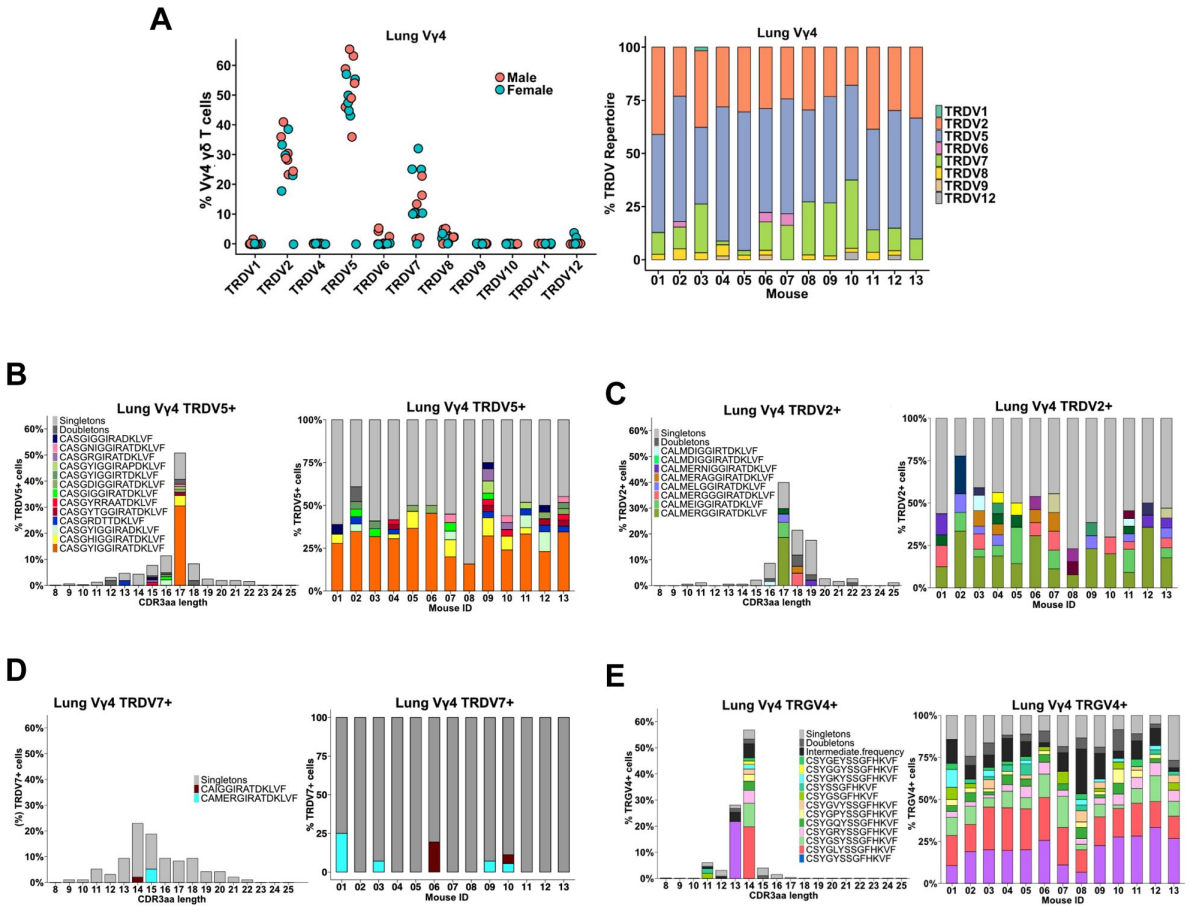

Supplemental Figure 9

Lung Vγ4 exhibit a high usage of TRDV7 chains with a diverse CDR3.

(A) TRDV usage among FACS-sorted lung Vγ4 γδ T cells from 7 male and 6 female mice. **(B)** *Left,* amino acid length distribution of top lung TRDV5^{+} CDR3δ clonotypes in the lung Vγ4 γδ T cell population. *Right*, distribution of the most frequent clonotypes among individual B6 mice. **(C)** *Left,* amino acid length distribution of top lung TRDV2^{+} CDR3δ clonotypes in the lung Vγ4 γδ T cell population. *Right*, distribution of the most frequent clonotypes among individual B6 mice. **(D)** *Left,* amino acid length distribution of top lung TRDV7^{+} CDR3δ clonotypes in the lung Vγ4 γδ T cell population. *Right*, distribution of the most frequent clonotypes among individual B6 mice. **(E)** *Left,* amino acid length distribution of top lung TRGV4^{+} CDR3γ clonotypes in the lung Vγ4 γδ T cell population. *Right*, distribution of the most frequent clonotypes among individual B6 mice.

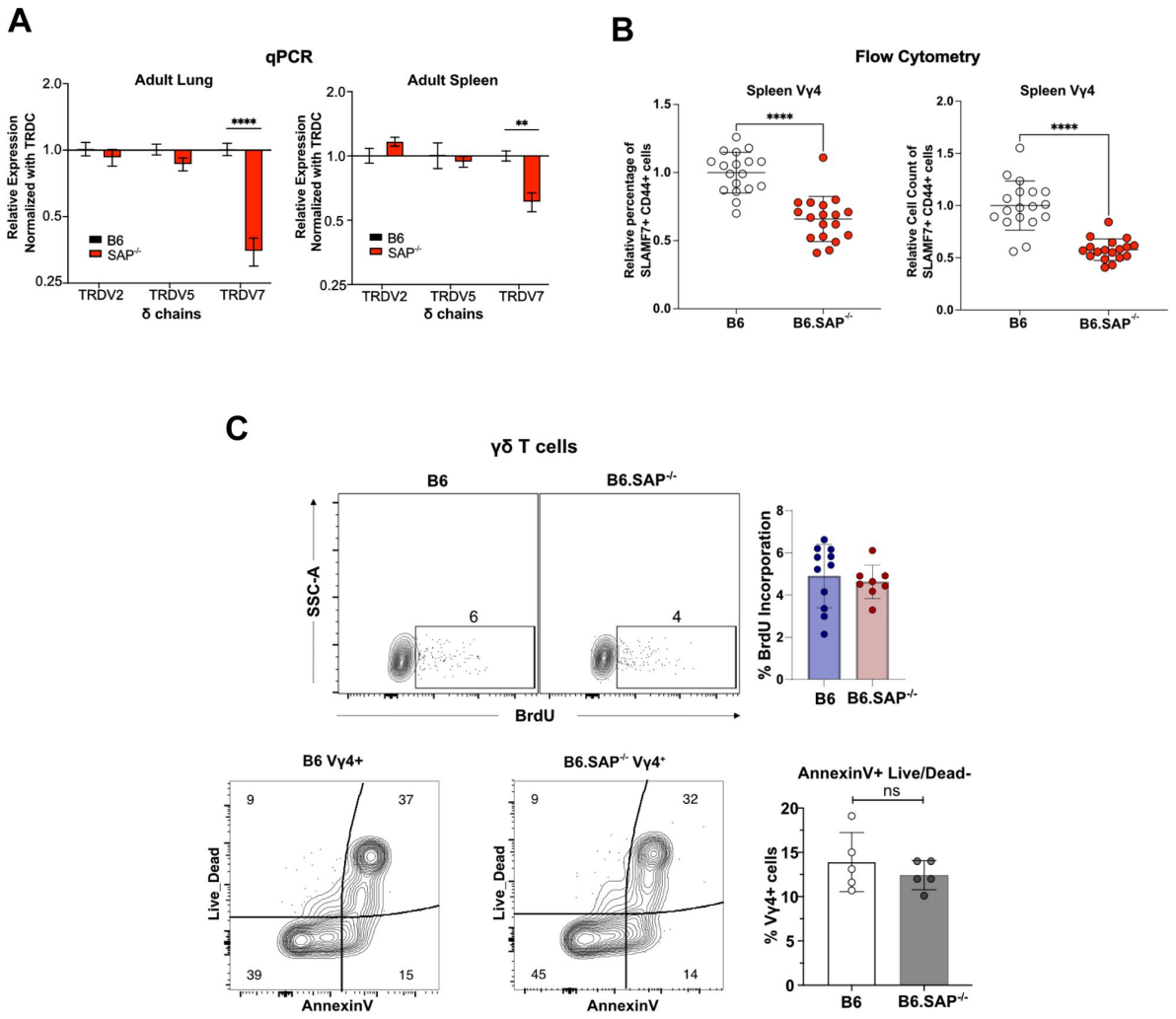

Supplemental Figure 10

Significant and specific reduction in peripheral TRGV4/TRDV7^{+} γδT1 in B6.SAP$^{-/-}$ mice.

(A) The relative expression of the specified TRDV transcripts in adult lung and spleen CD45^{+} leukocytes (normalized to total TRDC transcript levels) in B6 and B6.SAP$^{-/-}$ mice, **p < 0.01, ****p < 0.0001, two-way ANOVA followed by Sidak multiple-comparisons test. **(B)** SAP-dependent decrease in CD44^{+}SLAMF7^{+} spleen Vγ4 T cells. The relative percentage and count of CD44^{+}SLAMF7^{+} Vγ4 cells in B6 and B6.SAP$^{-/-}$ spleen subsets are shown. Data are representative of five independent experiments with 3-5 mice per strain per experiment, ****p, <0.0001, as determined by unpaired t tests. **(C)** No difference in lung Vγ4 homeostasis in B6.SAP$^{-/-}$ mice. *Top left,* Representative contour plots showing the frequency of BrdU staining in B6 and B6.SAP$^{-/-}$ lung γδ T cells. Cumulative data from two independent experiments are shown at *top right*. *Bottom left,* representative contour plots depicting Annexin V and Live/Dead staining in B6 and B6.SAP$^{-/-}$ lung γδ T cells. Cumulative results are shown at *bottom right,* and are representative of 3 independent experiments.

References

1. Grigoriadou K, Boucontet L, Pereira P (2003) **Most IL-4-producing gamma delta thymocytes of adult mice originate from fetal precursors** *J Immunol* **171**:2413–2420

2. Haas JD, et al. (2012) **Development of interleukin-17-producing gammadelta T cells is restricted to a functional embryonic wave** *Immunity* **37**:48–59

3. Ribot JC, et al. (2009) **CD27 is a thymic determinant of the balance between interferon-gamma- and interleukin 17-producing gammadelta T cell subsets** *Nat Immunol* **10**:427–436

4. Sumaria N, Grandjean CL, Silva-Santos B, Pennington DJ (2017) **Strong TCRgammadelta Signaling Prohibits Thymic Development of IL-17A-Secreting gammadelta T Cells** *Cell Rep* **19**:2469–2476

5. Chien YH, Zeng X, Prinz I (2013) **The natural and the inducible: interleukin (IL)-17-producing gammadelta T cells** *Trends Immunol* **34**:151–154

6. He W, et al. (2010) **Naturally activated V gamma 4 gamma delta T cells play a protective role in tumor immunity through expression of eomesodermin** *J Immunol* **185**:126–133

7. Gao Y, et al. (2003) **Gamma delta T cells provide an early source of interferon gamma in tumor immunity** *J Exp Med* **198**:433–442

8. Girardi M, et al. (2001) **Regulation of cutaneous malignancy by gammadelta T cells** *Science* **294**:605–609

9. Coffelt SB, et al. (2015) **IL-17-producing gammadelta T cells and neutrophils conspire to promote breast cancer metastasis** *Nature* **522**:345–348

10. Wu P, et al. (2014) **gammadeltaT17 cells promote the accumulation and expansion of myeloid-derived suppressor cells in human colorectal cancer** *Immunity* **40**:785–800

11. Rei M, et al. (2014) **Murine CD27(-) Vgamma6(+) gammadelta T cells producing IL-17A promote ovarian cancer growth via mobilization of protumor small peritoneal macrophages** *Proc Natl Acad Sci U S A* **111**:E3562–3570

12. Wakita D, et al. (2010) **Tumor-infiltrating IL-17-producing gammadelta T cells support the progression of tumor by promoting angiogenesis** *Eur J Immunol* **40**:1927–1937

13. Turchinovich G, Hayday AC (2011) **Skint-1 identifies a common molecular mechanism for the development of interferon-gamma-secreting versus interleukin-17-secreting gammadelta T cells** *Immunity* **35**:59–68

14. Jensen KD, et al. (2008) **Thymic selection determines gammadelta T cell effector fate: antigen-naive cells make interleukin-17 and antigen-experienced cells make interferon gamma** *Immunity* **29**:90–100

15. Munoz-Ruiz M, et al. (2016) **TCR signal strength controls thymic differentiation of discrete proinflammatory gammadelta T cell subsets** *Nat Immunol*

16. Chen ELY, Lee CR, Thompson PK, Wiest DL, Anderson MK, Zuniga-Pflucker JC (2021) **Ontogenic timing, T cell receptor signal strength, and Notch signaling direct gammadelta T cell functional differentiation in vivo** *Cell Rep* **35**

17. Kreslavsky T, et al. (2009) **TCR-inducible PLZF transcription factor required for innate phenotype of a subset of gammadelta T cells with restricted TCR diversity** *Proc Natl Acad Sci U S A* **106**:12453–12458

18. Spidale NA, et al. (2018) **Interleukin-17 Producing gammadelta T Cells Originate from SOX13(+) Progenitors that Are Independent of gammadeltaTCR Signaling** *Immunity*

19. Laird SM, Tuckerman EM, Cork BA, Linjawi S, Blakemore AI, Li TC (2003) **A review of immune cells and molecules in women with recurrent miscarriage** *Hum Reprod Update* **9**:163–174

20. Sumaria N, Martin S, Pennington Daniel J (2021) **Constrained TCRγδ-associated Syk activity engages PI3K to facilitate thymic development of IL-17A–secreting γδ T cells** *Science Signaling* **14**

21. Muro R, Nitta T, Nakano K, Okamura T, Takayanagi H, Suzuki H (2018) **gammadeltaTCR recruits the Syk/PI3K axis to drive proinflammatory differentiation program** *J Clin Invest* **128**:415–426

22. Cannons JL, Tangye SG, Schwartzberg PL (2011) **SLAM family receptors and SAP adaptors in immunity** *Annu Rev Immunol* **29**:665–705

23. Nichols KE, et al. (2005) **Regulation of NKT cell development by SAP, the protein defective in XLP** *Nat Med* **11**:340–345

24. Dienz O, et al. (2020) **Critical Role for SLAM/SAP Signaling in the Thymic Developmental Programming of IL-17- and IFN-gamma-Producing gammadelta T Cells** *J Immunol*

25. Legoux F, Gilet J, Procopio E, Echasserieau K, Bernardeau K, Lantz O (2019) **Molecular mechanisms of lineage decisions in metabolite-specific T cells** *Nat Immunol* **20**:1244–1255

26. Koay HF, et al. (2019) **A divergent transcriptional landscape underpins the development and functional branching of MAIT cells** *Sci Immunol* **4**

27. Azuara V, Levraud JP, Lembezat MP, Pereira P (1997) **A novel subset of adult gamma delta thymocytes that secretes a distinct pattern of cytokines and expresses a very restricted T cell receptor repertoire** *Eur J Immunol* **27**:544–553

28. Havran WL, Allison JP (1988) **Developmentally ordered appearance of thymocytes expressing different T-cell antigen receptors** *Nature* **335**:443–445

29. O'Brien RL, Born WK (2010) **gammadelta T cell subsets: a link between TCR and function?** *Semin Immunol* **22**:193–198

30. Stoeckius M, et al. (2017) **Simultaneous epitope and transcriptome measurement in single cells** *Nature methods* **14**:865–868

31. Coffey F, et al. (2014) **The TCR ligand-inducible expression of CD73 marks gammadelta lineage commitment and a metastable intermediate in effector specification** *J Exp Med* **211**:329–343

32. In TSH, et al. (2017) **HEB is required for the specification of fetal IL-17-producing gammadelta T cells** *Nat Commun* **8**

33. Satija R, Farrell JA, Gennert D, Schier AF, Regev A (2015) **Spatial reconstruction of single-cell gene expression data** *Nat Biotechnol* **33**:495–502

34. Havran WL, Chien YH, Allison JP (1991) **Recognition of self antigens by skin-derived T cells with invariant gamma delta antigen receptors** *Science* **252**:1430–1432

35. Itohara S, et al. (1990) **Homing of a gamma delta thymocyte subset with homogeneous T-cell receptors to mucosal epithelia** *Nature* **343**:754–757

36. Wencker M, et al. (2014) **Innate-like T cells straddle innate and adaptive immunity by altering antigen-receptor responsiveness** *Nat Immunol* **15**:80–87

37. Buus TB, Odum N, Geisler C, Lauritsen JPH (2017) **Three distinct developmental pathways for adaptive and two IFN-gamma-producing gammadelta T subsets in adult thymus** *Nat Commun* **8**

38. Xu H, et al. (2010) **MS4a4B, a CD20 homologue in T cells, inhibits T cell propagation by modulation of cell cycle** *PloS one* **5**

39. Howie D, et al. (2009) **MS4A4B is a GITR-associated membrane adapter, expressed by regulatory T cells, which modulates T cell activation** *J Immunol* **183**:4197–4204

40. Sagar, et al. (2020) **Deciphering the regulatory landscape of fetal and adult gammadelta T-cell development at single-cell resolution** *EMBO J* **39**

41. Laird RM, Laky K, Hayes SM (2010) **Unexpected role for the B cell-specific Src family kinase B lymphoid kinase in the development of IL-17-producing gammadelta T cells** *J Immunol* **185**:6518–6527

42. Zuberbuehler MK, et al. (2019) **The transcription factor c-Maf is essential for the commitment of IL-17-producing gammadelta T cells** *Nat Immunol* **20**:73–85

43. Narayan K, et al. (2012) **Intrathymic programming of effector fates in three molecularly distinct gammadelta T cell subtypes** *Nat Immunol* **13**:511–518

44. Lu Y, Cao X, Zhang X, Kovalovsky D (2015) **PLZF Controls the Development of Fetal-Derived IL-17+Vgamma6+ gammadelta T Cells** *J Immunol* **195**:4273–4281

45. Jojic V, et al. (2013) **Identification of transcriptional regulators in the mouse immune system** *Nat Immunol* **14**:633–643

46. Malhotra N, et al. (2013) **A network of high-mobility group box transcription factors programs innate interleukin-17 production** *Immunity* **38**:681–693

47. He Q, et al. (2022) **TOX deficiency facilitates the differentiation of IL-17A-producing gammadelta T cells to drive autoimmune hepatitis** *Cellular & molecular immunology* **19**:1102–1116

48. Fahl SP, et al. (2021) **The E protein-TCF1 axis controls gammadelta T cell development and effector fate** *Cell Rep* **34**

49. DiToro D, et al. (2020) **Insulin-Like Growth Factors Are Key Regulators of T Helper 17 Regulatory T Cell Balance in Autoimmunity** *Immunity* **52**:650–667

50. Roberts NA, et al. (2012) **Rank signaling links the development of invariant gammadelta T cell progenitors and Aire(+) medullary epithelium** *Immunity* **36**:427–437

51. Wei YL, et al. (2015) **A Highly Focused Antigen Receptor Repertoire Characterizes gammadelta T Cells That are Poised to Make IL-17 Rapidly in Naive Animals** *Frontiers in immunology* **6**

52. Kashani E, et al. (2015) **A clonotypic Vgamma4Jgamma1/Vdelta5Ddelta2Jdelta1 innate gammadelta T-cell population restricted to the CCR6(+)CD27(-) subset** *Nat Commun* **6**

53. Sim GK, Augustin A (1990) **Dominantly inherited expression of BID, an invariant undiversified T cell receptor delta chain** *Cell* **61**:397–405

54. Scaramuzzino S, et al. (2022) **Single-cell transcriptomics uncovers an instructive T-cell receptor role in adult gammadelta T-cell lineage commitment** *EMBO J* **41**

55. Prinz I, Sansoni A, Kissenpfennig A, Ardouin L, Malissen M, Malissen B (2006) **Visualization of the earliest steps of gammadelta T cell development in the adult thymus** *Nat Immunol* **7**:995–1003

56. Mingueneau M, et al. (2013) **The transcriptional landscape of alphabeta T cell differentiation** *Nat Immunol* **14**:619–632

57. Passoni L, et al. (1997) **Intrathymic delta selection events in gammadelta cell development** *Immunity* **7**:83–95

58. Kang J, Coles M, Cado D, Raulet DH (1998) **The developmental fate of T cells is critically influenced by TCRgammadelta expression** *Immunity* **8**:427–438

59. Haks MC, et al. (2005) **Attenuation of gammadeltaTCR signaling efficiently diverts thymocytes to the alphabeta lineage** *Immunity* **22**:595–606

60. Laird RM, Hayes SM (2010) **Roles of the Src tyrosine kinases Lck and Fyn in regulating gammadeltaTCR signal strength** *PloS one* **5**

61. Griewank K, et al. (2007) **Homotypic interactions mediated by Slamf1 and Slamf6 receptors control NKT cell lineage development** *Immunity* **27**:751–762

62. Kreslavsky T, Garbe AI, Krueger A, von Boehmer H (2008) **T cell receptor-instructed alphabeta versus gammadelta lineage commitment revealed by single-cell analysis** *J Exp Med* **205**:1173–1186

63. Fahl SP, et al. (2018) **Role of a selecting ligand in shaping the murine gammadelta-TCR repertoire** *Proc Natl Acad Sci U S A* **115**:1889–1894

64. Verykokakis M, Boos MD, Bendelac A, Adams EJ, Pereira P, Kee BL (2010) **Inhibitor of DNA binding 3 limits development of murine slam-associated adaptor protein-dependent "innate" gammadelta T cells** *PloS one* **5**

65. Lu Y, et al. (2019) **SLAM receptors foster iNKT cell development by reducing TCR signal strength after positive selection** *Nat Immunol*

66. Davidson D, et al. (2004) **Genetic evidence linking SAP, the X-linked lymphoproliferative gene product, to Src-related kinase FynT in T(H)2 cytokine regulation** *Immunity* **21**:707–717

67. Chan B, et al. (2003) **SAP couples Fyn to SLAM immune receptors** *Nature cell biology* **5**:155–160

68. Simarro M, et al. (2004) **SAP increases FynT kinase activity and is required for phosphorylation of SLAM and Ly9** *Int Immunol* **16**:727–736

69. Katz G, Krummey SM, Larsen SE, Stinson JR, Snow AL (2014) **SAP facilitates recruitment and activation of LCK at NTB-A receptors during restimulation-induced cell death** *J Immunol* **192**:4202–4209

70. Hayes SM, Li L, Love PE (2005) **TCR signal strength influences alphabeta/gammadelta lineage fate** *Immunity* **22**:583–593

71. Oh S, et al. (2023) **Distinct subpopulations of DN1 thymocytes exhibit preferential gammadelta T lineage potential** *Frontiers in immunology* **14**

72. Snow AL, et al. (2009) **Restimulation-induced apoptosis of T cells is impaired in patients with X-linked lymphoproliferative disease caused by SAP deficiency** *J Clin Invest* **119**:2976–2989

73. Edwards SC, et al. (2020) **A population of proinflammatory T cells coexpresses alphabeta and gammadelta T cell receptors in mice and humans** *J Exp Med* **217**

74. Rigau M, et al. (2020) **Butyrophilin 2A1 is essential for phosphoantigen reactivity by gammadelta T cells** *Science* **367**

75. Melandri D, et al. (2018) **The gammadeltaTCR combines innate immunity with adaptive immunity by utilizing spatially distinct regions for agonist selection and antigen responsiveness** *Nat Immunol* **19**:1352–1365

76. Sperling AI, Decker DC, DiPaolo RJ, Stern DA, Shum A, Bluestone JA (1997) **Selective expansion of Vgamma2-Vdelta7 TCR gammadelta cells in C57BL/6 mice is postnatal and extrathymic** *J Immunol* **159**:86–91

77. Sim GK, Augustin A (1991) **Extrathymic positive selection of gamma delta T cells. V gamma 4J gamma 1 rearrangements with "GxYS" junctions** *J Immunol* **146**:2439–2445

78. Van Gassen S, et al. (2015) **FlowSOM: Using self-organizing maps for visualization and interpretation of cytometry data** *Cytometry Part A : the journal of the International Society for Analytical Cytology* **87**:636–645

79. Ewels P, Magnusson M, Lundin S, Käller M (2016) **MultiQC: summarize analysis results for multiple tools and samples in a single report** *Bioinformatics (Oxford, England)* **32**

80. Martin M (2011) **Cutadapt removes adapter sequences from high-throughput sequencing reads** *EMBnet.journal* **17**

81. Patro R, Duggal G, Love MI, Irizarry RA, Kingsford C (2017) **Salmon provides fast and bias-aware quantification of transcript expression** *Nature methods* **14**:417–419

82. Soneson C, Love MI, Robinson MD (2015) **Differential analyses for RNA-seq: transcript-level estimates improve gene-level inferences** *F1000Research* **4**

83. Love MI, Huber W, Anders S (2014) **Moderated estimation of fold change and dispersion for RNA-seq data with DESeq2** *Genome biology* **15**

84. Zheng GXY, et al. (2017) **Massively parallel digital transcriptional profiling of single cells** *Nature Communications* **8**:1–12

85. Hao Y, et al. (2021) **Integrated analysis of multimodal single-cell data** *Cell* **184**:3573–3587

86. Denisenko E, et al. (2020) **Systematic assessment of tissue dissociation and storage biases in single-cell and single-nucleus RNA-seq workflows** *Genome biology* **21**

87. Stoeckius M, et al. (2018) **Cell Hashing with barcoded antibodies enables multiplexing and doublet detection for single cell genomics** *Genome biology* **19**

88. Hafemeister C, Satija R (2019) **Normalization and variance stabilization of single-cell RNA-seq data using regularized negative binomial regression** *Genome biology* **20**

89. Marsh SE (2021) **Marsh SE. scCustomize: Custom Visualizations & Functions for Streamlined Analyses of Single Cell Sequencing.) (2021).**

90. Squair JW, et al. (2021) **Confronting false discoveries in single-cell differential expression** *Nat Commun* **12**

91. Wolf FA, et al. (2019) **PAGA: graph abstraction reconciles clustering with trajectory inference through a topology preserving map of single cells** *Genome biology* **20**

92. Wolf FA, Angerer P, Theis FJ (2018) **SCANPY: large-scale single-cell gene expression data analysis** *Genome biology* **19**

93. Lefranc MP (2011) **IMGT, the International ImMunoGeneTics Information System** *Cold Spring Harb Protoc* **2011**:595–603

94. Pereira P, Boucontet L (2004) **Rates of recombination and chain pair biases greatly influence the primary gammadelta TCR repertoire in the thymus of adult mice** *J Immunol* **173**:3261–3270

95. Shugay M, et al. (2015) **VDJtools: Unifying Post-analysis of T Cell Receptor Repertoires** *PLoS Computational Biology* **11**

96. Ye J, Ma N, Madden TL, Ostell JM (2013) **IgBLAST: an immunoglobulin variable domain sequence analysis tool** *Nucleic Acids Res* **41**

Editors

Reviewing Editor
Shiny Nair
Yale University, New Haven, United States of America

Senior Editor
Satyajit Rath
Indian Institute of Science Education and Research (IISER), Pune, India

Reviewer #1 (Public Review):

Summary:
In this study the authors advance their previous findings on the role of the SLAM-SAP signaling pathway in the development and function of multiple innate-like gamma-delta T cell subsets. Using high throughput single cell proteogenomics approach, the authors uncover SAP-dependent developmental checkpoints, and the role of SAP signaling in regulating the diversion of γδ T cells into the αβ T cell developmental pathway. Finally, the authors define TRGV4/TRAV13-4(DV7)-expressing T cells as a novel, SAP-dependent Vγ4 γδT1 subset.

Strengths:
This study furthers our understanding of the importance and complexity of the SLAM-SAP signaling pathway not only in the development of innate-like γδ T cells but also the how it potentially balances the γδ/αβ T cell lineage commitment. Additionally, this study reveals the role of SAP-dependent events in generation of γδ TCR repertoire.

Comments on revised version:

The conclusions of the study are supported by well thought-out experiments and compelling data.

Weaknesses:
There are no major weakness in the study.

A few minor points:
(1) In the subsets of the γδ T cells that exhibit reduced BLK expression in B6. SAP KO mice, have the authors examined the expression of Lck and/or Fyn?
(2) Does BLK directly associate with SLAM F1 and or SLAM F6 receptors?
(3) Given the emerging role of γδ T cells in host immunity, it will be useful if the authors add a discussion of how their findings are relevant in disease conditions such as in cancer.

The author has adequately addressed all the reviewers' comments.

https://doi.org/10.7554/eLife.97229.2.sa2

Reviewer #2 (Public Review):

Summary:
Mistri et al explore the role of SLAM-SAP signaling in the developmental programming of innate-like gd T cell subsets. Using proteo-genomics, they determined that abrogation of SLAM-SAP signaling altered that programming, reducing some IL-17 producing subsets, including a novel Vγ4 γδT1 subset, and diverting gdTCR-expressing precursors to the ab fate. Altogether, this is a very thorough, thoughtfully interpreted study that adds significantly to our understanding of the contribution of the SLAM-SAP pathway to lineage specification. A

particularly interesting element is the role of SLAM-SAP in preventing gd17 progenitors from switching fates and adopting the ab fate.

Comments on revised version:

The authors have addressed the minor issues raised in the original submission.

https://doi.org/10.7554/eLife.97229.2.sa1

Author response:

The following is the authors' response to the original reviews.

> ***Reviewer #1:***
>
> *(1) In the subsets of the γδ T cells that exhibit reduced BLK expression in B6. SAP KO mice, have the authors examined the expression of Lck and/or Fyn?*

The reviewer raises an excellent point. We have included in the revised manuscript additional data on Lck and Fyn expression in our scRNAseq dataset in (new Suppl. Fig. 1 and new Suppl. Fig. 4). These data revealed that in contrast to Blk, which appears primarily restricted to the γδT17 clusters, Lck and Fyn exhibit a much broader distribution and lack restriction to specific clusters. We did note that, like Blk, Lck and Fyn transcripts were abundant in SAP-dependent C2 cluster cells. Pseudobulk analysis on the immature clusters revealed that, neither Fyn nor Lck expression level differences reached our cut-off of 0.5 log2 FC (log2 FC Blk = 1.06), leading us to conclude that Blk is particularly dependent on SAP. We did note, however, that the magnitude of Lck differential expression was close to the 0.5 log2 FC cut-off and that its expression was increased in B6.SAP-/- γδ T cells (Suppl. Fig. 4). These results have been added to lines 202-212 in the Results section and lines 491-499 in the Discussion section.

> *(2) Does BLK directly associate with SLAM F1 and or SLAM F6 receptors?*

The reviewer raises an interesting question given previous reports that BLK, LCK, and FYN have all been implicated in γδ T cell development. While SAP has a well-known ability to recruit FYN to SLAMF1 and there is evidence of a similar SAP-mediated recruitment of LCK to SLAMF6, we are not aware of any evidence a SAP-BLK interaction or of a direct binding of BLK to SLAM family receptors. Future experiments to investigate this possiibility are certainly warranted. In the revised ms, we have included additional discussion of these possibilities (lines 491- 499).

> *(3) Given the emerging role of γδ T cells in host immunity, it would be useful if the authors could add a discussion of how their findings are relevant in disease conditions such as cancer.*

We agree and have included new text in the Introduction (lines 37-45).

> *(4) Delete repeated words in lines 546 and line 553.*

Thank you—this has been corrected in the revised manuscript.

> ***Reviewer #2:***
>
> *This is a very complete study and requires no additional experimentation. One thing to keep in mind in assessing the ultimate fate of the "ab wannabe cells" is that mechanisms*

> *exist to silence the gd TCR as cells differentiate to the DP stage and so their presence as diverted DP cells may not be evident by staining for gdTCR expression - and will only be evident transcriptomically.*

We appreciate this helpful comment from the reviewer which we will take into consideration in our future experimental design.

> *There are a couple of minor points to raise:*
>
> *(1) Figure 3C is not called out in the text.*

Thank you—this has been corrected in the revised manuscript.

> *(2) Line 546 - "dependent" is repeated.*

Thank you—this has been corrected in the revised manuscript.

https://doi.org/10.7554/eLife.97229.2.sa0